Table 1. Cellular genes differentially expressed in hepatitis C virus (HCV) core transgenic mouse liver

	Upregulated	Downregulated
Lipid metabolism	NPC1 Catalase Very long chain acyl-CoA dehydrogenase Carboxylesterase selenoprotein P Carbonic anhydrase Adipose differentiation-related protein Bilirubin/phenol family UDP glucuronosyltransferase	Stearoyl-CoA desaturase Sterol-carrier protein X Alpha-enolase carnitine acetyltransferase Gal beta 1,4(3) GlcNAc alpha 2,3-sialyltransferase Very long chain acyl-CoA synthetase Liver transferrin 4-Hydroxyphenylpyruvate dioxygenase LAF1 transketolase *s*-Adenosylmethionine synthetase Apolipoprotein A-II
Transcription and cell proliferation	Int-6 GCN5L1 *H. sapiens* 8.2k-Da differentiation factor USF1 Initiation factor eIF-4AI Human elongation factor-1-delta Sui1	Human guanine nucleotide regulatory protein Alpha-fetoprotein Retinol binding protein
Inflammation	Alpha-1 protease inhibitor 3 Hemopexin	Alpha-2-macroglobulin LMW prekininogen Complement component C3 AHSG(alpha 2 HS-glycoprotein) homologue
Others	Microvascular endothelial differentiation gene 1 Diazepam-binding inhibitor Argininosuccinate synthetase Skeletal muscle alpha-tropomyosin Ampd3 gene DNA-binding protein	Vitronectin Epithelin 1 and 2 Murinoglobulin

microsomal triglyceride transfer protein (MTP) by HCV core protein[26]; this inhibits the secretion of very low density protein (VLDL) from the liver, yielding an increase of triglycerides in the liver. The last pathway involves sterol regulatory element-binding protein (SREBP)-1c, which regulates the production of triglycerides and phospholipids. In HCV core gene transgenic mice, SREBP-1c is activated, whereas neither SREBP-2 nor SREBP-1a is upregulated.[27]

In relation to lipid metabolism, the core protein has also been found to interact with retinoid X receptor (RXR)-α.[28] RXR-α is one of the nuclear receptors, which forms a homodimer or heterodimers with other nuclear receptors, including PPAR (peroxisome proliferator-activated receptor)-α, and plays a pivotal role in the regulation of the expression of genes relating to lipid metabolism, cell differentiation, and proliferation. In fact, the core protein of HCV activates genes that have an RXR-α-responsive element as well as those with a PPAR-α-responsive element, both in mice and in cultured cells.[28] Based on these results, we, then, examined the expression and function of PPAR-α in the liver of core gene transgenic mice.

PPAR-α activation in HCV-associated hepatocarcinogenesis

PPAR-α, one of the PPAR genes, plays a central role as a heterodimer with RXR-α in regulating fatty acid transport and catabolism. It is also known as a molecular target for lipid-lowering fibrate drugs.[29] On the other hand, prolonged administration of PPAR-α agonists causes HCC in rodents. Currently, there is little evidence that the low-affinity fibrate ligands are associated with human cancers, but it is possible that chronic activation of high-affinity ligands could be carcinogenic in humans.[29]

The level of PPAR-α protein was increased in the liver of core gene transgenic mice as early as 9 months of age. PPAR-α protein is accumulated with age in the nuclei of hepatocytes together with cyclin D1 protein. However, the level of PPAR-α mRNA was not increased at any age. By pulse-chase experiment, the stability of nuclear PPAR-α was increased in the presence of the core protein. In line with the increase of PPAR-α protein, target genes of PPAR-α were activated in the liver of core gene transgenic mice; these genes include

cyclin D1, cyclin-dependent kinase (CDK)-4, acy-CoA oxidase, and peroxisome thiolase.[30] However, in general, the activation of PPAR-α leads to improvement but not aggravation of steatosis. Then, what is the function of PPAR-α activation that is observed in the core gene transgenic mice?

To clarify the role of PPAR-α activation in pathogenesis of steatosis and HCC, we mated a core gene transgenic mouse with a PPAR-α knockout (KO) mouse and studied the phenotype. PPAR-α KO mice have reduced expression of target genes of PPAR-α, and have mild steatosis in the liver, as expected.[31] It was unanticipated, however, that steatosis was absent in PPAR-α-null or -heterozygous core gene transgenic mice but present in PPAR-α-intact core gene transgenic mice at the age of 9 or 24 months.[30] 8-Hydroxy deoxyguanosine (8-OHdG) and peroxylipids, both of which are markers for oxidative stress, were decreased in PPAR-α KO core gene transgenic mice. Mitochondrial dysfunction in the core gene transgenic mice, which contributes to overproduction of oxidative stress,[19] was also improved in PPAR-α KO core gene transgenic mice.

Finally, PPAR-α KO core gene transgenic mice did not develop HCC at the age of 24 months, whereas about one-third of PPAR-α-intact core gene transgenic mice did. It should be noted that core gene transgenic mice that are heterozygous for the PPAR-α gene also did not develop HCC.[32] When clofibrate, a peroxisome proliferator, was administered for 24 months to PPAR-α-heterozygous mice, either with or without the core gene, HCC developed in a higher rate in the core gene (+) mice with greater PPAR-α activation. It should be noted that steatosis was present only in core gene (+) PPAR-α-heterozygous mice. In summary, steatosis and HCC developed in PPAR-α-intact but not in PPAR-α-heterozygous or PPAR-α-null core gene transgenic mice, indicating that not the presence but the persistent activation of PPAR-α would be important in hepatocarcinogenesis by HCV core protein. In general, PPAR-α acts to ameliorate steatosis, but with the presence of mitochondrial dysfunction, which is also provoked by the core protein, the core-activated PPAR-α may exacerbate steatosis. Persistent activation of PPAR-α with "strong" ligands such as the core protein of HCV could be carcinogenic in humans, although the low-affinity fibrate ligands are not likely associated with human cancers.

HCV core protein causes "fatty acid spiral"

Figure 2 illustrates our current hypothesis for the role of lipid metabolism in HCV-associated hepatocarcinogenesis. Immune-mediated inflammation should also play a pivotal role in hepatocarcinogenesis in HCV infection. However, in HCV infection, the core protein induces steatosis through the aforementioned pathways, leading to "fatty acid spiral" in the presence of the mitochondrial complex 1 dysfunction and PPAR-α activation, both of which are caused by the core protein. These intracellular alterations would contribute to hepatocarcinogenesis by inducing oxidative stress overproduction and cell-growth signal activation. In such a sense, the core protein of HCV is not a classical-type oncoprotein, but rather seems to contribute to hepatocarcinogenesis by modulating intracellular metabolism and signaling.

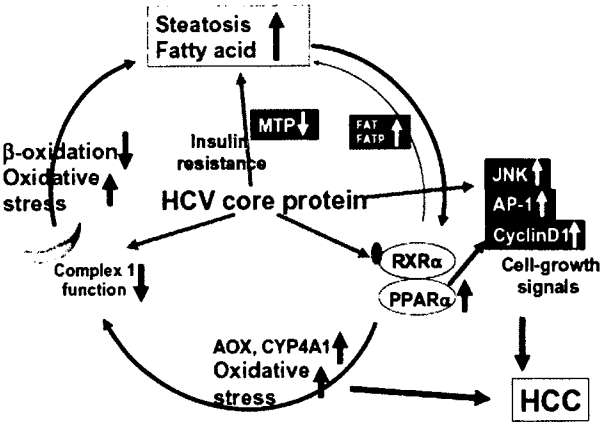

Fig. 2. "Fatty acid spiral" by HCV core protein. In HCV infection, the core protein induces steatosis via several pathways, leading to "fatty acid spiral" in the presence of the mitochondrial complex 1 dysfunction and PPAR-α activation, both of which are also caused by the core protein. These intracellular alterations would contribute to hepatocarcinogenesis by inducing oxidative stress overproduction and cell-growth signal activation. In such a sense, the core protein of HCV is not a classical type oncoprotein, but rather seems to contribute to hepatocarcinogenesis by modulating intracellular metabolism and signaling. *HCV*, hepatitis C virus; *HCC*, hepatocellular carcinoma; *ROS*, reactive oxygen species; *JNK*, c-Jun N-terminal kinase; *ERK*, extracellular signal-regulated kinase; *AP-1*, activating protein-1; *RXR-α*, retinoid X receptor-α; *PPAR-α*, peroxisome proliferator activated receptor-α; *AOX*, acyl-CoA oxidase; *CYP*, cytochrome P450; *MTP*, microsomal triglyceride transfer protein; *FAT*, fatty acid translocase; fatty acid transport protein

The HCV protein may allow some steps in multistep hepatocarcinogenesis to be skipped

The results of our studies on transgenic mice have indicated a carcinogenic potential of the HCV core protein in vivo; thus, HCV would be directly involved in hepatocarcinogenesis. In research studies of carcinogenesis, the theory outlined by Kinzler and Vogelstein[33] has gained wide popularity. They have proposed that the

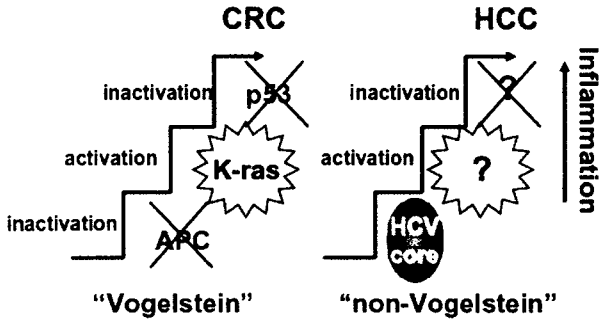

Fig. 3. Mechanism of HCV-associated hepatocarcinogenesis. Multiple steps are required in the induction of all cancers; it would be mandatory for hepatocarcinogenesis that genetic mutations accumulate in hepatocytes. However, in HCV infection, some of these steps may be skipped in the development of HCC in the presence of the core protein. The overall effects achieved by the expression of the core protein would be the induction of HCC, even in the absence of a complete set of genetic aberrations required for carcinogenesis. By considering such a "non-Vogelstein-type" process for the induction of HCC, a plausible explanation may be given for many unusual events happening in HCV carriers

development of colorectal cancer is induced by the accumulation of a complete set of cellular gene mutations. They have deduced that mutations in the APC gene for inactivation, those in K-*ras* for activation, and those in the p53 gene for inactivation accumulate, which cooperate toward the development of colorectal cancer.[33] Their theory has been extended to the carcinogenesis of other cancers as well, called "Vogelstein-type" carcinogenesis (Fig. 3).

On the basis of the results we obtained for the induction of HCC by the HCV core protein, we would like to introduce a different mechanism for hepatocarcinogenesis in HCV infection. We do allow multistages in the induction of all cancers; it would be mandatory for hepatocarcinogenesis that many mutations accumulate in hepatocytes. Some of these steps, however, may be skipped in the development of HCC in HCV infection to which the core protein would contribute (see Fig. 3). The overall effect achieved by the expression of the viral protein would be the induction of HCC, even in the absence of a complete set of genetic aberrations required for carcinogenesis.

By considering such a "non-Vogelstein-type" process for the induction of HCC, a plausible explanation may be given for many unusual events happening in HCV carriers.[34] Now it does not seem so difficult as before to determine why HCC develops in persistent HCV infection at an outstandingly high incidence. Our theory may also give an account of the nonmetastatic and multicentric de novo occurrence characteristics of HCC, which would be the result of persistent HCV infection.

References

1. Saito I, Miyamura T, Ohbayashi A, Harada H, Katayama T, Kikuchi S, et al. Hepatitis C virus infection is associated with the development of hepatocellular carcinoma. Proc Natl Acad Sci USA 1990;87:6547–9.
2. Ikeda K, Saitoh S, Suzuki Y, Kobayashi M, Tsubota A, Koida I, et al. Disease progression and hepatocellular carcinogenesis in patients with chronic viral hepatitis: a prospective observation of 2215 patients. J Hepatol 1998;28:930–8.
3. Okuse C, Yotsuyanagi H, Koike K. Hepatitis C as a systemic disease: virus and host immunologic responses underlie hepatic and extrahepatic manifestations. J Gastroenterol 2007;42:857–65.
4. Koike K, Moriya K. Metabolic aspects of hepatitis C: steatohepatitis distinct from NASH. J Gastroenterol 2005;40:329–36.
5. Negro F. Insulin resistance and HCV: will new knowledge modify clinical management? J Hepatol 2006;45:514–9.
6. Powell EE, Jonsson JR, Clouston AD. Steatosis: co-factor in other liver diseases. Hepatology 2005;42:5–13.
7. Kiyosawa K, Sodeyama T, Tanaka E, Gibo Y, Yoshizawa K, Nakano Y, et al. Interrelationship of blood transfusion, non-A, non-B hepatitis and hepatocellular carcinoma: analysis by detection of antibody to hepatitis C virus. Hepatology 1990;12:671–5.
8. Yotsuyanagi H, Shintani Y, Moriya K, Fujie H, Tsutsumi T, Kato T, et al. Virological analysis of non-B, non-C hepatocellular carcinoma in Japan: frequent involvement of hepatitis B virus. J Infect Dis 2000;181:1920–8.
9. Moriya K, Yotsuyanagi H, Shintani Y, Fujie H, Ishibashi K, Matsuura Y, et al. Hepatitis C virus core protein induces hepatic steatosis in transgenic mice. J Gen Virol 1997;78:1527–31.
10. Moriya K, Fujie H, Shintani Y, Yotsuyanagi H, Tsutsumi T, Matsuura Y, et al. Hepatitis C virus core protein induces hepatocellular carcinoma in transgenic mice. Nat Med 1998;4:1065–8.
11. Koike K, Moriya K, Ishibashi K, Matsuura Y, Suzuki T, Saito I, et al. Expression of hepatitis C virus envelope proteins in transgenic mice. J Gen Virol 1995;76:3031–8.
12. Koike K, Moriya K, Yotsuyanagi H, Shintani Y, Fujie H, Ishibashi K, et al. Sialadenitis resembling Sjögren's syndrome in mice transgenic for hepatitis C virus envelope genes. Proc Natl Acad Sci USA 1997;94:233–6.
13. Bach N, Thung SN, Schaffner F. The histological features of chronic hepatitis C and autoimmune chronic hepatitis: a comparative analysis. Hepatology 1992;15:572–7.
14. Lerat H, Honda M, Beard MR, Loesch K, Sun J, Yang Y, et al. Steatosis and liver cancer in transgenic mice expressing the structural and nonstructural proteins of hepatitis C virus. Gastroenterology 2002;122:352–65.
15. Naas T, Ghorbani M, Alvarez-Maya I, Lapner M, Kothary R, De Repentigny Y, et al. Characterization of liver histopathology in a transgenic mouse model expressing genotype 1a hepatitis C virus core and envelope proteins 1 and 2. J Gen Virol 2005;86:2185–96.
16. Machida K, Cheng KT, Lai CK, Jeng KS, Sung VM, Lai MM. Hepatitis C virus triggers mitochondrial permeability transition with production of reactive oxygen species, leading to DNA damage and STAT3 activation. J Virol 2006;80:7199–207.
17. Moriya K, Fujie H, Yotsuyanagi H, Shintani Y, Tsutsumi T, Matsuura Y, et al. Subcellular localization of hepatitis C virus structural proteins expressed in transgenic liver. Jpn J Med Sci Biol 1997;50:169–77.
18. Sasaki Y. Does oxidative stress participate in the development of hepatocellular carcinoma? J Gastroenterol 2006;41:1135–48.
19. Moriya K, Nakagawa K, Santa T, Shintani Y, Fujie H, Miyoshi H, et al. Oxidative stress in the absence of inflammation in a mouse model for hepatitis C virus-associated hepatocellular carcinogenesis. Cancer Res 2001;61:4365–70.

20. Moriya K, Todoroki T, Tsutsumi T, Fujie H, Shintani Y, Miyoshi H, et al. Increase in the concentration of carbon 18 monounsaturated fatty acids in the liver with hepatitis C: analysis in transgenic mice and humans. Biophys Biochem Res Commun 2001;281: 1207–12.
21. Okuda M, Li K, Beard MR, Showalter LA, Scholle F, Lemon SM, Weinman SA. Mitochondrial injury, oxidative stress, and antioxidant gene expression are induced by hepatitis C virus core protein. Gastroenterology 2002;122:366–75.
22. Tsutsumi T, Suzuki T, Moriya K, Yotsuyanagi H, Shintani Y, Fujie H, et al. Intrahepatic cytokine expression and AP-1 activation in mice transgenic for hepatitis C virus core protein. Virology 2002;304:415–24.
23. Tsutsumi T, Suzuki T, Moriya K, Shintani Y, Fujie H, Miyoshi H, et al. Hepatitis C virus core protein activates ERK and p38 MAPK in cooperation with ethanol in transgenic mice. Hepatology 2003;38:820–8.
24. Miyamoto H, Moriishi K, Moriya K, Murata S, Tanaka K, Suzuki T, et al. Hepatitis C virus core protein induces insulin resistance through a PA28γ-dependent pathway. J Virol 2007;81:1727–35.
25. Shintani Y, Fujie H, Miyoshi H, Tsutsumi T, Kimura S, Moriya K, et al. Hepatitis C virus and diabetes: direct involvement of the virus in the development of insulin resistance. Gastroenterology 2004;126:840–8.
26. Perlemuter G, Sabile A, Letteron P, Vona G, Topilco A, Koike K, et al. Hepatitis C virus core protein inhibits microsomal triglyceride transfer protein activity and very low density lipoprotein secretion: a model of viral-related steatosis. FASEB J 2002; 16:185–94.
27. Moriishi K, Mochizuki R, Moriya K, Miyamoto H, Mori Y, Abe T, et al. Critical role of PA28γ in hepatitis C virus-associated steatogenesis and hepatocarcinogenesis. Proc Natl Acad Sci USA 2007;104:1661–6.
28. Tsutsumi T, Suzuki T, Shimoike T, Moriya K, Yotsuyanagi H, Matsuura Y, et al. Interaction of hepatitis C virus core protein with retinoid X receptor-α modulates its transcriptional activity. Hepatology 2002;35:937–46.
29. Peters JM, Cheung C, Gonzalez FJ. Peroxisome proliferator-activated receptor-alpha and liver cancer: where do we stand? J Mol Med 2005;83:774–85.
30. Tanaka N, Moriya K, Kiyosawa K, Koike K, Aoyama T. Hepatitis C virus core protein induces spontaneous and persistent activation of peroxisome proliferator-activated receptor alpha in transgenic mice: implications for HCV-associated hepatocarcinogenesis. Int J Cancer 2008;122:124–31.
31. Akiyama TE, Sakai S, Lambert G, Nicol CJ, Matsusue K, Pimprale S, et al. Conditional disruption of the peroxisome proliferator-activated receptor gamma gene in mice results in lowered expression of ABCA1, ABCG1, and apoE in macrophages and reduced cholesterol efflux. Mol Cell Biol 2002;22: 2607–19.
32. Tanaka N, Moriya K, Kiyosawa K, Koike K, Gonzalez FJ, Aoyama T. PPAR-α is essential for severe hepatic steatosis and hepatocellular carcinoma induced by HCV core protein. J Clin Invest 2008;118:683–94.
33. Kinzler KW, Vogelstein B. Lessons from hereditary colorectal cancer. Cell 1996;87:159–70.
34. Koike K. Molecular basis of hepatitis C virus-associated hepatocarcinogenesis: lessons from animal model studies. Clin Gastroenterol Hepatol 2005;3:S132–5.

Research Article **Chromatography**

Received: 31 July 2008, Revised: 7 August 2008, Accepted: 7 August 2008 Published online in Wiley Interscience: 2008

(www.interscience.wiley.com) DOI 10.1002/bmc.1139

Limitation of immunoaffinity column for the removal of abundant proteins from plasma in quantitative plasma proteomics

Tomoko Ichibangase,[a] Kyoji Moriya,[b] Kazuhiko Koike[b] and Kazuhiro Imai[a]*

ABSTRACT: In plasma proteomics, before a proteome analysis, it is essential to prepare protein samples without high-abundance proteins, including albumin, via specific preparation techniques, such as immunoaffinity capture. However, our preliminary experiments suggested that functional changes with use alter the ability of the immunoaffinity column. Thus, in this study, to evaluate the changes of the removal ability of abundant proteins from plasma by the immunoaffinity column, plasma proteome analysis was performed for the long-term test for the reproducibility of the affinity column using the fluorogenic derivatization–liquid chromatography–tandem mass spectrometry method combined with an IgY column. The specific adsorption for albumin decreased with an increase in the number of the column usage before its expiration date. Moreover, it was demonstrated that hydrophobic high molecular weight compounds in plasma adsorbed onto the column materials surface contributed to the functional changes from specific immunoaffinity adsorption into hydrophobic interaction. These results suggested that, in quantitative plasma proteomics studies, it is important to keep in mind the risk of not only the nonselective loss but also the changes in the adsorption ability of the immunoafinity column. Copyright © 2008 John Wiley & Sons, Ltd.

Keywords: plasma; proteomics; immunoaffinity column; abundant protein; FD-LC-MS/MS method

Introduction

Blood samples can be taken at a particular point in time with little burden on patients and the constituents of the blood samples could reflect a developing or existing illness because tissue-specific proteins may be released into the brood stream from the damaged or dead cells. Therefore, it is generally recognized in proteomics studies that blood samples represent the greatest potential source of information on the proteins related to human diseases. However, plasma proteome analysis aiming at quantitative protein profiling and biomarker discovery is not easily done. Since several high-abundance proteins, such as albumin, typically constitute greater than 90% of total protein mass, the detection of lower-abundance proteins which presumably are the biologically interesting population is interfered with by the dominant proteins. To address the complexity of these samples, it is essential to prepare samples via specific preparation techniques to remove high-abundance proteins from the samples before the proteome analysis (Linke *et al.*, 2007; Martosella *et al.*, 2005; Qian *et al.*, 2006; Steel *et al.*, 2003). There are a number of approaches for removing proteins based on their biochemical and biophysical features, such as molecular weight, mass, density, hydrophobicity, surface change and isoelectric point. Among these techniques, immunoaffinity capture using antibodies is rapidly becoming the prefractionation method of choice in proteomics analysis. Commercial kits using an avian immunoglobulin yolk (IgY) have recently become available due to its high avidity and lesser cross-reactivity with heterologous human proteins (Huang *et al.*, 2005; Linke *et al.*, 2007; Qian *et al.*, 2006). A number of researchers have already indicated its utility and the improvement of the detection of low-abundance proteins by the elimination of the high-abundance proteins using the IgY affinity column (Gong *et al.*, 2006; Huang *et al.*, 2005; Linke *et al.*, 2007; Liu *et al.*, 2006; Qian *et al.*, 2006).

We have recently developed a highly sensitive and quantitative proteomics method called fluorogenic derivatization–liquid chromatography–tandem mass spectrometry (FD-LC-MS/MS) (Masuda *et al.*, 2004; Toriumi and Imai, 2003). The method consists of separation of the fluorogenic derivatized proteins by high-performance liquid chromatography (HPLC), isolation of the target protein obtained by HPLC, hydrolysis and identification of the target protein by LC-MS/MS with the probability-based protein identification algorithm. This highly selective, sensitive and reproducible method enables the post-translational proteins and isoforms to be distinguished. The method was applied to the extracts of *Caenorhabditis elegans*, mousee liver and breast cancer cell lines, and revealed the proteins related to early-stage Parkinson's

* Correspondence to: K. Imai, Research Institute of Pharmaceutical Sciences, Musashino University, 1-1-20 Shinmachi, Nishitokyo-shi, Tokyo 202-8585, Japan. E-mail: k-imai@musashino-u.ac.jp

[a] Research Institute of Pharmaceutical Sciences, Musashino University, Tokyo, Japan

[b] Department of Internal Medicine, Graduate school of Medicine, University of Tokyo, Tokyo, Japan

Abbreviations used: DAABD-Cl, 7-Chloro-*N*-[2-(dimethylamino)ethyl]-2,1,3-benzoxadiazole-4-sulfonamide; FD, fluorogenic derivatization; HCCA, α-cyano-4-hydroxycinnamic acid; TCEP, Tris (2-carboxyethyl) phosphine hydrochloride; TFA, trifluoroacetic acid; TOF, time-of-flight.

Contract/grant sponsor: MEXT HAITEKU (2004–2008), Grant-in-Aid for Young Scientists (Start-up).

Contract/grant sponsor: Mochida Memorial Foundation for Medical and Pharmaceutical Research.

disease (Ichibangase *et al.*, 2008), hepatocarcinogenesis (Ichibangase *et al.*, 2007) and tumor progression and metastasis (Imai *et al.*, 2008). During the course of our studies, we applied the FD-LC-MS/MS method to plasma proteomics. To detect plasma biomarkers that are probably masked by the high-abundant proteins, an IgY affinity column was utilized for the removal of the dominant proteins, such as albumin, from plasma before the fluorogenic derivatization (FD) of the plasma proteins. On the preliminary experiments, the quantitative changes of the peaks on the chromatograms obtained from the same samples were observed on every occasion of sample treatment with the affinity column. Since the detectability of the fluorogenic derivatized proteins by the HPLC-fluorescence detector is always constant, the change in the removal ability of the IgY column for the abundant proteins could be monitored during the usage of the column. Although it was reported that there was a risk of loss by inadvertent capture of low-abundance proteins (Bjorhall *et al.*, 2005; Gong *et al.*, 2006; Linke *et al.*, 2007; Plavina *et al.*, 2007; Yocum *et al.*, 2005), there are no reports of long-term tests for the reproducibility of the affinity column in quantitative proteome analysis.

In this study, to evaluate the removal ability of abundant proteins from plasma by the affinity column, we performed proteome analysis of plasma sample and protein standards by FD-LC-MS/MS combined with the IgY technique and investigated the cause of the quantitative changes of the chromatograms mentioned above.

Experimental

Materials and Methods

Reagents. 7-Chloro-*N*-[2-(dimethylamino)ethyl]-2,1,3-benzoxadiazole-4-sulfonamide (DAABD-Cl) and 6.0 M guanidine hydrochloride (pH 8.7 buffer solution) were purchased from Tokyo Chemical Industry (Tokyo, Japan). Ethylenediamine-*N*,*N*,*N*′,*N*′-tetraacetic acid sodium salt (Na_2EDTA) and 3-[(3-Cholamidopropyl) dimethyammonio]-1-propanesulfonate (CHAPS) were from Dojindo Laboratories (Kumamoto, Japan). Tris (2-carboxyethyl) phosphine hydrochloride (TCEP) was obtained from Sigma-Aldrich (St Louis, MO, USA). Acetonitrile and trifluoroacetic acid (TFA) for the HPLC-fluorescence detection were HPLC grade and were obtained from Wako Pure Chemical Industries (Osaka, Japan). All other reagents used were of analytical grade.

Affinity Columns

The prepacked IgY-R7 Spin Column and Seppro®-IgY12 were obtained from Beckman Coluter (Fullerton, CA, USA) and GenWay Bioteck (San Diago, CA, USA), respectively. The IgY-R7 Spin Column (1.2 mL spin column) removes seven high-abundance proteins in rodent plasma (albumin, IgG, α2-antitrypsin, IgM, transferring, haptoglobin and fibrinogen) and utilizes centrifugation as the force for affinity separation. The column is said to be reusable 100 times under proper conditions. The Seppro®-IgY12 column is optimized for human plasma and removes 12 high-abundance proteins (IgA, α1-acid glycoprotein, α2-macroglobin, apolipoproteins A-I and apolipoproteins A-II besides the above seven proteins). This column is used with the high-throughput automated proteomic sample processing instrument (Magtration System SA-1; Precision System Science, Chiba, Japan) and is said to be able to be used 30 times. Both companies are corporate partners for the exclusive marketing of the IgY microbeads technology, and both column materials are the same except for recognized animal species to the IgY.

Plasma Samples

For the IgY-R7 Spin Column, plasma sample were obtained from C57BL/6N male mice (10 and 19 months; Clea Japan, Tokyo, Japan) by centrifugation at 5510 rpm for 10 min at 4°C, and frozen at –80°C until use. On the other hand, the human control plasma sample purchased from Sigma-Aldrich was used for the Seppro®-IgY12 column. The control plasma sample was passed through a 0.45 μm filter before use.

Treatment of Mouse Plasma with the IgY-R7 Spin Column

Mouse plasma treated with the spin column was carried out according to the manufacturer-instructed column usage and loading capacity [10 μL plasma diluted with dilution/washing buffer: 10 mM Tris–HCl, 150 mM NaCl, pH 7.4 (TBS)]. Three buffers (dilution/washing buffer; stripping buffer: 100 mM glycine, pH 2.5; neutralization buffer: 100 mM Tris–HCl, pH 8.0) were used under the separation scheme that consisted of sample loading–washing–eluting–neutralization followed by a re-equilibration scheme for a total cycle time of 40 min. To increase the recovery of the non-specific proteins, the resulting flow-though fraction and the washing fractions were collected and concentrated to 10 μL with 3.0 kDa molecular weight cutoff device according to the manufacturer's instructions (Microcon YM-3; Millipore, Billerica, MA, USA).

Treatment of Protein Standards and Control Human Plasma Sample with the Seppro®-IgY12 Column

The molecular weight standards, consisting of phosphorylase B, serum albumin, ovalbumin, carbonic anhydrase, trypsin inhibitor and lysozyme for electrophoresis (Table 1; 12 mg/mL protein amount; low range; Bio-Rad, Herccules, CA, USA), were employed in sample processing without dilution to evaluate the recovery of non-specific proteins from the column. The injected amount of the protein standards was 2.4 mg protein per injection to the affinity column. Since, in the instructions, 15 μL of plasma (generally corresponding to 70–80 mg proteins/mL) was diluted to 500 μL and loaded to the affinity column, the injected amount of the standards was compatible. According to the manufacturer's instructions, the protein standards were set in the sample holding and then the flow-though fraction was obtained.

The control human plasma sample was also treated according to the manual. Briefly, 15 μL of plasma sample was diluted with the dilution/washing buffer to 500 μL, and the sample was set in the sample holding, as in the case of the protein standards. The resulting flow-though fraction of the plasma was concentrated

Table 1. Protein standards and the number of labeled region with DAABD-Cl

Protein	Source	MW (kDa)	No. of rabeled region
Phosphorylase B	Rabbit muscle	97.4	10
Serum albumin	Bovine	66.2	35
Ovalbumin	Hen egg white	45	5
Carbonic anhydrase	Bovine	31	2
Trypsin inhibitor	Soybean	21.5	5
Lysozyme	Hen egg white	14.4	6

to 15 μL with a Microcon YM-3 device. A series cycle including the sample loading–washing–eluting–neutralization finished in 65 min.

FD-LC-MS/MS Conditions

Each FD condition was optimized for the protein standards and for plasma samples in order to obtain the highest peak on the chromatograms. For the protein standards, a 2.5 μL aliquot of the flow-though fraction was mixed with 30 μL of a mixture of 0.83 mM TCEP, 3.3 mM Na_2EDTA and 16.6 mM CHAPS in the pH 8.7 buffer solution, 12.5 μL of the buffer solution and 5.0 μL of 8.0 mM DAABD-Cl in acetonitrile. The mixture was reacted at 50°C for 5.0 min, and the reaction was stopped with 1.5 μL of 20% TFA. A 20 μL aliquot of the above reaction mixture was injected to the HPLC system (Hitachi L-2000 series; Hitachi Instruments, Tokyo, Japan) using a column of Intrada WP-RP (30 nm pore size, 250 × 4.6 mm i.d., Imtakt Co, Kyoto, Japan) at 60°C with a flow rate of 0.55 mL/min. The eluent (A) and eluent (B) were water–acetonitrile–TFA (90:10:0.15, v/v/v) and water–acetonitrile–TFA (30:70:0.05, v/v/v), respectively. The gradient condition was established from 5 to 100% eluent (B) over a period of 60 min. For mouse and control plasma samples, a 6.0 μL aliquot of the flow-though fraction was mixed with 30 μL of the above mixture of TCEP, Na_2EDTA and CHAPS, 10 μL of the buffer solution and 4.0 μL of 825 mM DAABD-Cl in dioxane. After the FD reaction (50°C for 5.0 min), the reaction was stopped with 2.0 μL of 20% TFA. An aliquot (10 μL) of the reaction mixture was injected, and the longer column (Intrada WP-RP 30 nm pore size, 500 × 4.6 mm i.d., Imtakt Co) together with a precolumn (Intrada WP-RP 30 nm pore size, 5.0 × 2.0 mm i.d., Imtakt Co) at 60°C was adopted with a flow rate of 0.55 mL/min on the HPLC system. The mobile phases consisted of water–acetonitrile–TFA (A) 90:10:0.15 and (B) 30:70:0.05. Mobile phase (C) was the same as (A), except with 0.05% TFA. The gradient condition is described in Fig. 1. Fluorescence detection was carried out at 395 and 505 nm for the excitation and emission wavelengths, respectively. The peak height of each protein peak obtained from the HPLC chromatograms was calculated by HITACHI EZChrom Elite™ Chromatography Data System (Hitachi Instruments) and the identification of the standard proteins was accomplished according to the previous report (Ichibangase *et al.*, 2007).

Scanning Electron Microscopy and Matrix-assisted Laser Desorption/Ionization MS Analysis

Scanning electron microscopy (SEM) and matrix-assisted laser desorption/ionization (MALDI) MS analyses were conducted in Jeol Datum (Tokyo, Japan) and Bruker Daltonics Japan (Kanagawa, Japan), respectively.

For SEM analysis, the column materials were diluted with phosphate buffer (300 mOsm) and fixed with fixative (2.5% glutaraldehyde in PBS, pH 7.0) for 10 min. The fixed sample was captured on the filter (SEM-Pore: 0.6 μm i.d.; 10 μm) and washed with the buffer. After the osmium-fix (2% OsO_4) and a brief rinse with the fixative solutions, specimens were dehydrated in a series of graded ethanol (30–100%). The immersed specimens in ethanol were replaced with isoamyl phenylacetate and subjected to critical point drying. The dried samples were coated with osmium using a plasma coater (OPC80N, Jeol). Images were acquired using a Jeol JSM-7401F in normal SEM mode. For the low power microscope images for the whole picture of a material, a lower electron image (LEI) was applied.

For MALDI MS analysis, the column materials were washed and spotted on a plate. α-Cyano-4-hydroxycinnamic acid (HCCA) was used as matrix. MALDI mass spectra were acquired with time-of-flight (TOF) MS (autoflex III, Bruker Daltonics) in positive linear mode.

Results and Discussion

Quantitative Functional Changes of the IgY-R7 Spin Column after a Number of Treatments with Mouse Plasma

For the detection of low-abundance proteins in mouse plasma, the removal of high-abundance proteins from mouse plasma with the affinity column was performed prior to the FD-LC-MS/MS proteome analysis. Typical chromatograms are shown in Fig. 1(A), obtained from the same mouse plasma sample treated with 80 and 86 cycles of the same spin column, respectively. All peak heights obtained from the 86 cycles of the spin column were clearly higher compared with those obtained from the 80 cycles. Although a difference between column lots might exist, there were also significant differences in the removability of the affinity column between the second (column lot no. 2) and the 44th cycles (column lot no. 1) of the treated spin column [Fig. 1(B)]. The relative standard deviation (RSD) of the protein peaks was calculated between-day ($n = 3$) using samples provided by the same treatment number of the column. The RSD values were less than 21.6%, obtained from the peak in Fig. 1(A), suggesting that the detectability of the fluorogenic derivatized proteins by HPLC is constant. Therefore, it was considered that the quantitative changes of the peaks on the chromatograms might result from the changes in the affinity column by the sample treatment.

Evaluation of Seppro®-IgY12 Column for the Adsorption of Protein Standards using an Automatic Instrument

To eliminate a manual usage error from the sample processing, a high-throughput automated instrument, SA-1, for the removal of high-abundance proteins from human plasma samples with a Seppro®-IgY12 column was investigated. For the evaluation of the exact adsorption ratio of specific and non-specific proteins to the affinity column, the affinity column was periodically treated with protein standards after treatment with a control human plasma sample some dozen times. Since the other investigator has reported the non-specific adsorption of the protein by concentration methods such as a centrifugal filter to be about 15% (Linke *et al.*, 2007), the flow-through fraction of the injected protein standards from the affinity column was subjected directly to the FD-LC-MS/MS analysis without a protein concentration step in this study.

At first, to eliminate the non-specific adsorption to the affinity column, the protein standards mixture was divided into two parts and one was subjected into the untreated affinity column, and the flow-though fraction was derivatized with the fluorogenic reagent, DAABD-Cl, and separated by the HPLC system (4.8 μg protein/HPLC injection). Another part of the protein standards mixture was diluted and derivatized with DAABD-Cl, and injected onto the HPLC system (4.8 μg protein/HPLC injection). The obtained chromatograms are depicted in Fig. 2. Each protein peak was collected, digested in peptide mixtures, and identified by applying the peptides to HPLC-MS/MS with a

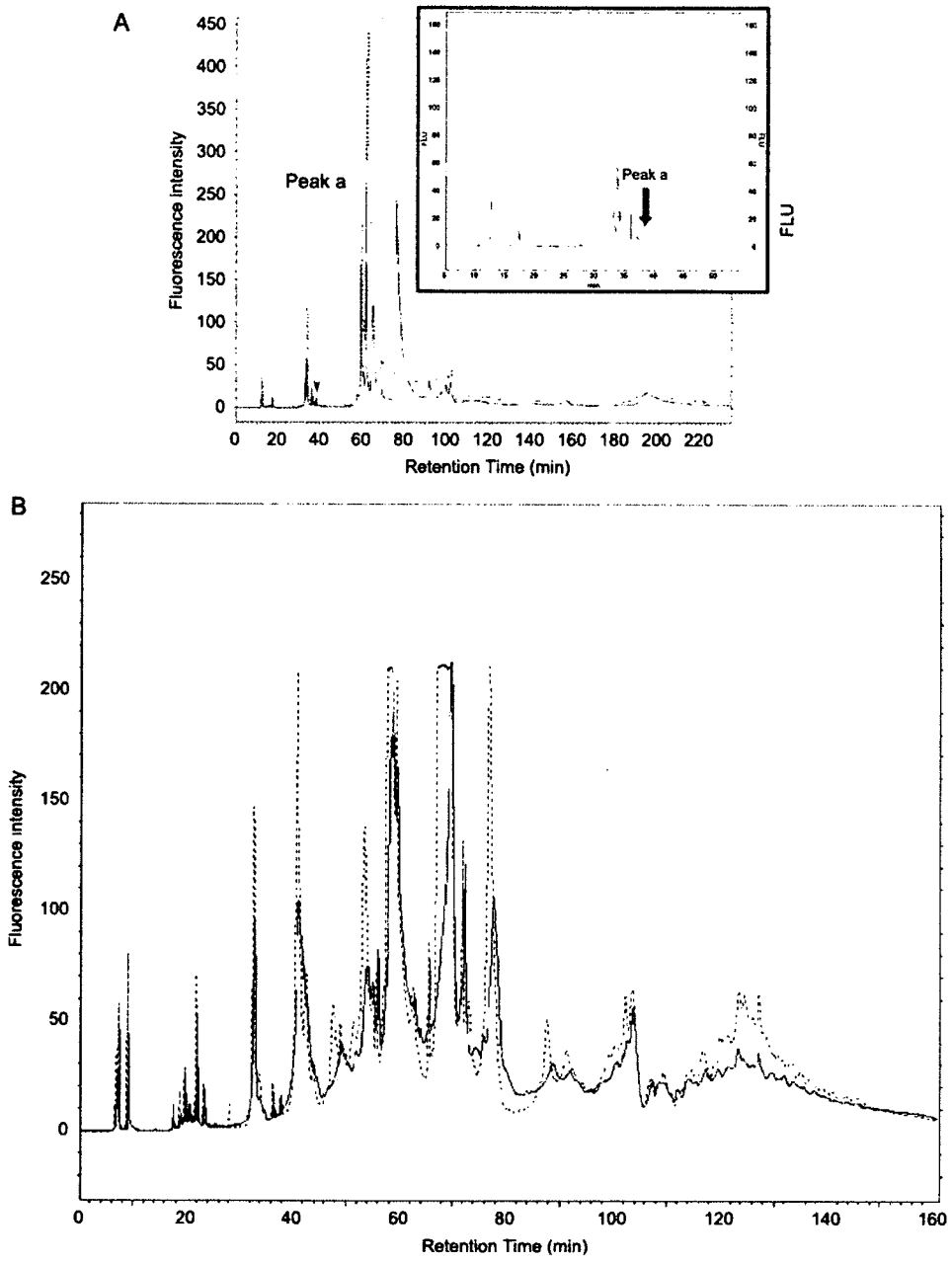

Figure 1. Chromatograms of mouse plasma samples treated with IgY-R7 Spin Columns. (A) The mouse plasma (19 months, C57BL/6N) treated 80 times (solid line) and 86 times (dotted line) in the same spin column. The gradient conditions were as follows: time (min), 0 → 10 → 20 → 44 → 48 → 68 → 80 → 90 → 108 → 120 → 130 → 160 → 180 → 230; B (%): 5 → 5 → 30 → 30 → 35 → 38 → 39.2 → 39.2 → 42 → 43 → 44 → 45 → 47 → 58; C (%): 0 → 0 → 0 → 0 → 0 → 0 → 0 → 60.8 → 58 → 57 → 56 → 55 → 53 → 42. (B) The mouse plasma samples (10 months, C57BL/6N) were treated with the second cycle (column lot no. 2; solid line) and the 44th cycle (column lot no. 1; dotted line) of each spin column. The gradient conditions were as follows: time (min), 0 → 5 → 10 → 22 → 24 → 34 → 54 → 60 → 60.1 → 80 → 130 → 140 → 150 → 160 → 170; B(%): 5 → 5 → 30 → 30 → 35 → 38 → 42 → 43 → 43 → 47 → 58 → 60 → 60 → 75 → 78; C(%): 0 → 0 → 0 → 0 → 0 → 0 → 0 → 0 → 57 → 53 → 42 → 40 → 40 → 25 → 22.

database-searching algorism. Table 2 shows the adsorption ratio of the proteins to the untreated column and the identified protein names. The protein names of peak 1 and 2 could not be identified since these peaks were peptides coexisting in the protein standards. Also, carbonic anhydrase and ovalbumin could not be detected. Since carbonic anhydrase has only two cycteine residue for labeling with DAABD-Cl, its detection might be difficult. The reason for the undetected ovalbumin was not clear. Since this study was aimed at investigating the changes in the adsorption of the specific and non-specific proteins using the column, this issue was not examined further. Consequently, although the affinity column was able to efficiently remove bovine serum

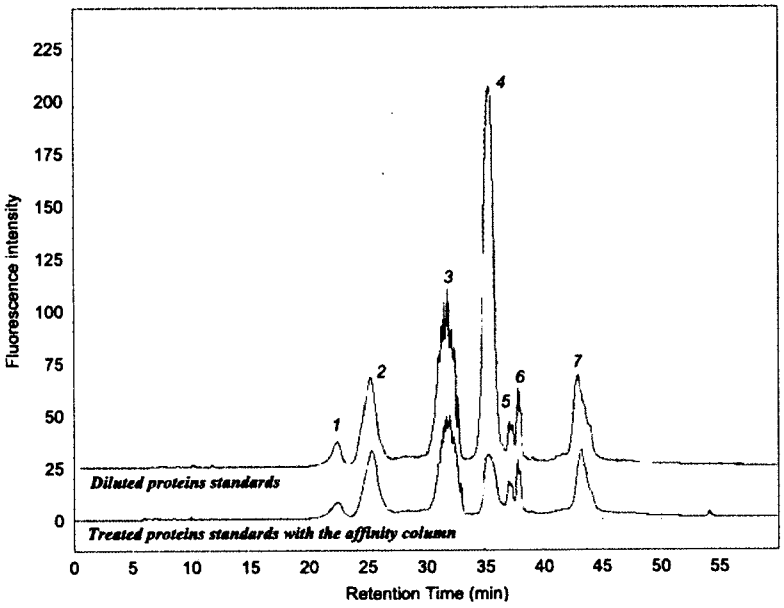

Figure 2. Chromatograms of the protein standards which were treated with Seppro®-IgY12 column and diluted to the same protein amount (4.8 μg/HPLC injection) as the amount for the column treatment. The peak numbers correspond to Table 2.

Table 2. Adsorption ratio to the untreated Seppro®-IgY12 column and protein names obtained by FD-LC-MS/MS method

Peak no.	Adsorption ratio to the untreated Seppro®-IgY12	Protein name
1	38.5%	Peptide
2	30.6%	Peptide
[a]3	45.9%	Lysozyme
4	83.9%	Bovine serum albumin (BSA)
[b]5	18.3%	Trypsin inhibitor
6	28.5%	Trypsin inhibitor
7	30.4%	Phosphorylase B

[a]3, [b]5: Most highest peak

albumin (BSA; 83.9%) as compared with the other proteins in the standards, non-specific binding to the column materials or to carrier proteins such as albumin itself was observed in the 18.3–45.9% range and could result in the loss of presumed biomarkers.

Next, the time series changes of the specific and non-specific adsorption of proteins to the column were investigated. The protein standards mixture was treated with the column periodically after 10 and 20 cycles of treatment of the control plasma sample. The relation of the changes of the protein standards adsorption to the number of uses of the affinity column is shown in Fig. 3(A). The specific adsorption of BSA decreased with an increase in the number of times the column was used. However, the non-specific adsorption for lysozyme, trypsin inhibitor and phosphorylase B reached a maximum at 11 cycles and decreased at 21 cycles. Since the affinity column was optimized for human plasma, the absorption of BSA for the column might be weaker than for plasma albumin. However, the adsorption of albumin in control plasma also decreased with an increase in the number of times the column was used (data not shown). Moreover, since the slopes of decrease differed among the protein standards, the correlation of each adsorption with molecular weight of each protein was calculated [Fig. 3(B)]. The open dots show the value of BSA in Fig. 3(B). The correlation coefficient value was the closest to 1.00 ($R^2 = 0.813$) for 21 cycles [Fig. 3(B-3)], demonstrating that the adsorption ability of the column does not depend any longer on the affinity of the antibody but on the hydrophobicity of the protein. In contrast, the correlation of the values obtained from the first cycle [Fig. 3(B-1); $R^2 = 0.077$] was not fairly observed between the adsorption ability and the hydrophobicity, and the value for BSA was apart from those for other proteins. Therefore, BSA was specifically removed as compared with the other protein standards by the immunoaffinity adsorption. Also, as shown in Fig. 3(B-2), the result obtained from 11 cycles ($R^2 = 0.012$) demonstrated that all proteins bound to the surface of the affinity column materials equally. Therefore, the present data demonstrates that the quantitative changes of the adsorption for the affinity column appear before the limited use of the column (30 times in the manufacturer's instructions).

Understanding the State of the Plasma-treated Column Materials

To understand the state of the column materials of the Seppro®-IgY12 column, the untreated and 11- and 21-times-treated column materials were subjected to electron microscopy and MALDI-TOF-MS analysis.

As shown in Fig. 4, the SEM images show an obvious difference between the untreated and treated materials. The attachment of the unknown bio-molecules to the materials surface appeared and increased with an increase in the number of treatments.

Next, in order to characterize the attached compounds, the same materials were subjected to MALDI-TOF-MS analysis. Since

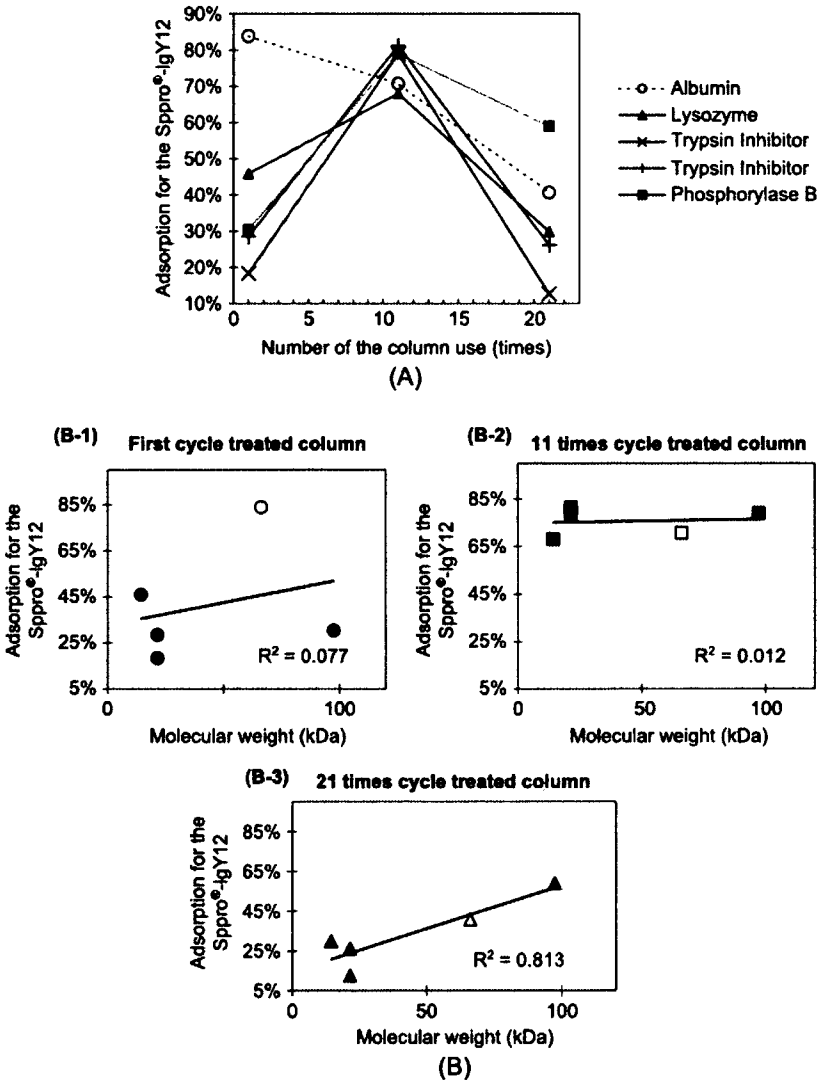

Figure 3. Changes of the adsorption ratio of protein standards for Seppro®-IgY12 column. (A) Relation of the adsorption ratio to the number of times the column was used. (B) Correlation of the adsorption ratio for the column with molecular weight of each protein standard using the column treater one (B-1), 11 (B-2) and 21 (B-3). The open dots show the value for BSA.

direct laser irradiation of the materials could affect the instrument, the positions to be irradiated were the points of the existence of many matrices on a few column materials. Although several peaks existed of less than 70,000 *m/z* in each mass spectrum, the higher molecular weight peaks (7266, 9689, 14,532 and 29,041 *m/z*) appeared in the treated but not in the untreated materials (Fig. 5). After the materials were washed with acetonitrile, the higher molecular weight peaks in the treated materials disappeared (data not shown). Therefore, the compounds attached to the material surface should be hydrophobic high-molecular-weight compounds existing in human plasma.

Two analyses of the column materials surface demonstrated that the hydrophobic high-molecular-weight compounds in plasma adsorbed onto the surface of the affinity column materials and contributed to the changes in the adsorption ability of plasma protein from immunoaffinity into hydrophobic interactions. Howevere, further studies are needed to characterize the exact details of the compounds.

Conclusions

To investigate the ability to remove abundant proteins from plasma by immnoaffinity using the IgY column, FD-LC-MS/MS method was applied to the long-term test of the reproducibility of the column. It was demonstrated that the immunoaffinity column was effective in removing BSA from the protein standards mixture, but, in addition, removing other proteins in the 18.3–45.0% range. The results suggested that the proteins of possible biomarkers could be lost and their quantification made difficult. Moreover, the specific adsorption of BSA in the protein standards mixture and of albumin in the control human plasma samples decreased with an increase in the number of times the column was used with both samples before its use expired. To examine the cause of the functional changes of the immunoaffinity, the correlations between the adsorption ratio for the affinity column and molecular weight of the adsorbed proteins were calculated, and the column materials surface was also investigated by SEM and

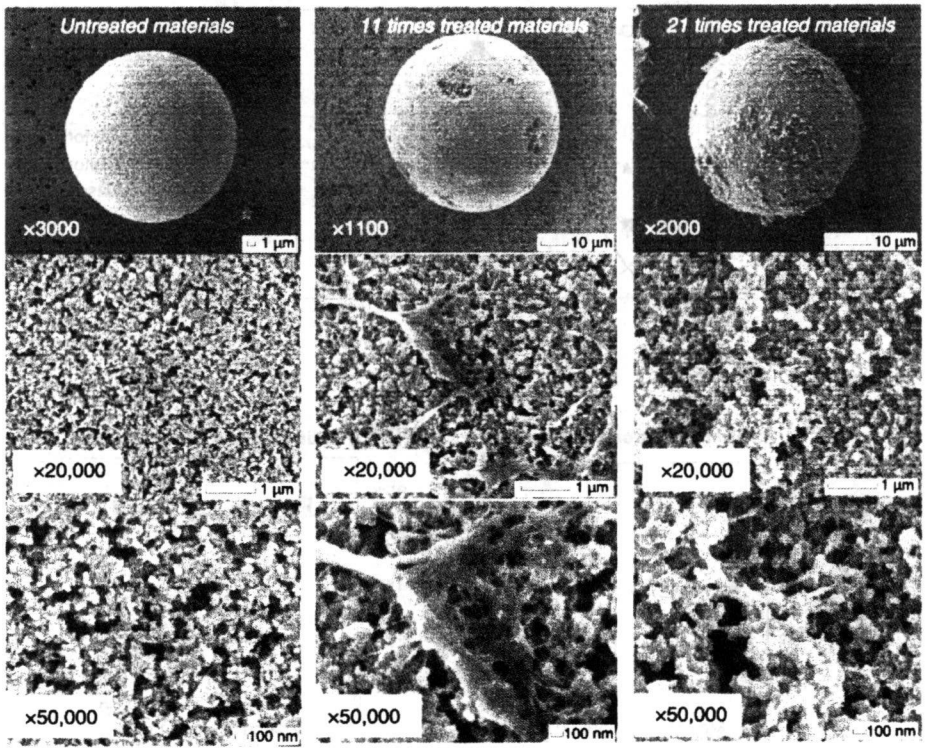

Figure 4. SEM images of the untreated and 11- and 21-times-treated column material surfaces. Magnification in SEM was controlled in a range of × 1100–3000 to show the whole picture of the material.

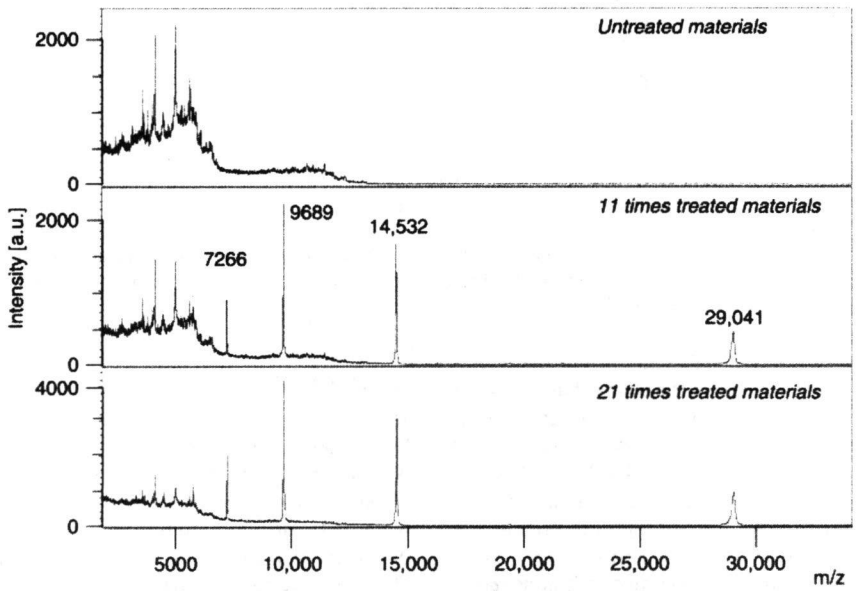

Figure 5. MALDI-TOF-mass spectrum of the untreated and 11- and 21-times-treated column material surface.

MALDI MS analysis. These data demonstrated the attachment of the hydrophobic high-molecular-weight compounds in plasma to the surface, suggesting that on every sample treatment with the affinity column, the adsorption ability of plasma protein changed into hydrophobic interactions. Further studies to characterize the attached compounds are required, and the elucidation of the compounds might lead to the improvement of the affinity column technique and contribute to progress in quantitative plasma proteomics.

Reproducibility is prerequisite for accurate quantitative proteome analysis of clinical samples for biomarker identification and quantification. For this purpose, it is generally essential to

prepare protein samples without high-abundance proteins via specific pre-fractionation techniques to enhance the detection of low-abundance proteins in plasma, and thus, immunoaffinity separation is now chosen as a reliable pre-fractionation method. However, this study indicated that, in quantitative plasma proteomics studies, it is important to keep in mind the risk of not only nonselective loss but also functional changes of the adsorption ability for the immunoaffinity column.

Acknowledgements

We would like to thank Precision System Science Co. Ltd for providing the high-throughput automated proteomic sample processing instrument, Magtration System SA-1, and Bruker Daltonics Japan for performing MALDI MS analysis of the affinity column materials. Part of this work was supported by a MEXT HAITEKU (2004–2008), Grant-in-Aid for Young Scientists (Start-up) and the Mochida Memorial Foundation for Medical and Pharmaceutical Research.

References

Bjorhall K, Miliotis T and Davidsson P. Comparison of different depletion strategies for improved resolution in proteomic analysis of human serum samples. *Proteomics* 2005; **5**: 307–317.

Gong Y, Li X, Yang B, Ying W, Li D, Zhang Y, Dai S, Cai Y, Wang J, He F and Xiaohong Q. Different immunoaffinity fractionation strategies to characterize the human plasma proteome. *Journal of Proteome Research* 2006; **5**: 1379–1387.

Huang L, Harvie G, Feitelson JS, Gramatikoff K, Herold DA, Allen DL, Amunngama R, Hagler RA, Pisano MR, Zhang WW and Xiangming F. Immunoaffinity separation of plasma proteins by IgY microbeads: meeting the needs of proteomic sample preparation and analysis. *Proteomics* 2005; **5**: 3314–3328.

Ichibangase T, Moriya K, Koike K and Imai K. A proteomics method revealing disease-related proteins in livers of hepatitis-infected mouse model. *Journal of Proteome Research* 2007; **6**: 2841–2849.

Ichibangase T, Saimaru H, Takamura N, Kuwahara T, Koyama A, Iwatsubo T and Imai K. Proteomics of Caenorhabditis elegans over-expressing human alpha-synuclein analyzed by fluorogenic derivatization-liquid chromatography/tandem mass spectrometry: identification of actin and several ribosomal proteins as negative markers at early Parkinson's disease stages. *Biomedical Chromatography* 2008; **22**: 232–234.

Imai K, Ichibangase T, Saitoh R and Hoshikawa Y. A proteomics study on human breast cancer cell lines by fluorogenic derivatization–liquid chromatography/tandem mass spectrometry *Biomedical Chromatography* 2008; **22**: 1303–1313.

Linke T, Doraiswamy S and Harrison EH. Rat plasma proteomics: effects of abundant protein depletion on proteomic analysis. *Journal of Chromatography B Analytical Technologies in the Biomedical and Life Dciences* 2007; **849**: 273–281.

Liu T, Qian WJ, Mottaz HM, Gritsenko MA, Norbeck AD, Moore RJ, Purvine SO, Camp DG and Smith RD. Evaluation of multiprotein immunoaffinity subtraction for plasma proteomics and candidate biomarker discovery using mass spectrometry. *Molecular and Cellular Proteomics* 2006; **5**: 2167–2174.

Martosella J, Zolotarjova N, Liu H, Nicol G and Boyes BE. Reversed-phase high-performance liquid chromatographic prefractionation of immunodepleted human serum proteins to enhance mass spectrometry identification of lower-abundant proteins. *Journal of Proteome Research* 2005; **4**: 1522–1537.

Masuda M, Toriumi C, Santa T and Imai K. Fluorogenic derivatization reagents suitable for isolation and identification of cysteine-containing proteins utilizing high-performance liquid chromatography–tandem mass spectrometry. *Analytical Chemistry* 2004; **76**: 728–735.

Plavina T, Wakshull E, Hancock WS and Hincapie M. Combination of abundant protein depletion and multi-lectin affinity chromatography (M-LAC) for plasma protein biomarker discovery. *Journal of Proteome Research* 2007; **6**: 662–671.

Qian WJ, Jacobs JM, Liu T, Camp DG and Smith RD. Advances and challenges in liquid chromatography–mass spectrometry-based proteomics profiling for clinical applications. *Molecular and Cellular Proteomics* 2006; **5**: 1727–1744.

Steel LF, Trotter MG, Nakajima PB, Mattu TS, Gonye G and Block T. Efficient and specific removal of albumin from human serum samples. *Molecular and Cellular Proteomics* 2003; **2**: 262–270.

Toriumi C and Imai K. An identification method for altered proteins in tissues utilizing fluorescence derivatization, liquid chromatography, tandem mass spectrometry, and a database-searching algorithm. *Analytical Chemistry* 2003; **75**: 3725–3730.

Yocum AK, Yu K, Oe T and Blair IA. Effect of immunoaffinity depletion of human serum during proteomic investigations. *Journal of Proteome Research* 2005; **4**: 1722–1731.

THE JOURNAL OF BIOLOGICAL CHEMISTRY VOL. 285, NO. 2, pp. 845–854, January 8, 2010

Ethanol Enhances Hepatitis C Virus Replication through Lipid Metabolism and Elevated NADH/NAD$^+$*

Received for publication, July 17, 2009, and in revised form, October 30, 2009 Published, JBC Papers in Press, November 12, 2009, DOI 10.1074/jbc.M109.045740

Scott Seronello[‡], Chieri Ito[‡], Takaji Wakita[§], and Jinah Choi[‡1]

From the [‡]School of Natural Sciences, University of California, Merced, Atwater, California 95343 and the [§]National Institute of Infectious Diseases, Tokyo 162-8640, Japan

Ethanol has been suggested to elevate HCV titer in patients and to increase HCV RNA in replicon cells, suggesting that HCV replication is increased in the presence and absence of the complete viral replication cycle, but the mechanisms remain unclear. In this study, we use Huh7 human hepatoma cells that naturally express comparable levels of CYP2E1 as human liver to demonstrate that ethanol, at subtoxic and physiologically relevant concentrations, enhances complete HCV replication. The viral RNA genome replication is affected for both genotypes 2a and 1b. Acetaldehyde, a major product of ethanol metabolism, likewise enhances HCV replication at physiological concentrations. The potentiation of HCV replication by ethanol is suppressed by inhibiting CYP2E1 or aldehyde dehydrogenase and requires an elevated NADH/NAD$^+$ ratio. In addition, acetate, isopropyl alcohol, and concentrations of acetone that occur in diabetics enhance HCV replication with corresponding increases in the NADH/NAD$^+$. Furthermore, inhibiting the host mevalonate pathway with lovastatin or fluvastatin and fatty acid synthesis with 5-(tetradecyloxy)-2-furoic acid or cerulenin significantly attenuates the enhancement of HCV replication by ethanol, acetaldehyde, acetone, as well as acetate, whereas inhibiting β-oxidation with β-mercaptopropionic acid increases HCV replication. Ethanol, acetaldehyde, acetone, and acetate increase the total intracellular cholesterol content, which is attenuated with lovastatin. In contrast, both endogenous and exogenous ROS suppress the replication of HCV genotype 2a, as previously shown with genotype 1b. Conclusion: Therefore, lipid metabolism and alteration of cellular NADH/NAD$^+$ ratio are likely to play a critical role in the potentiation of HCV replication by ethanol rather than oxidative stress.

Ethanol consumption is a well-known risk factor for chronic liver diseases. Ethanol is also a key cofactor in the pathogenesis induced by hepatitis C virus (HCV),[2] and it decreases the efficacy of anti-HCV treatments (1, 2). Likewise, HCV infection exacerbates liver damage caused by prolonged alcohol abuse (2). It has also been reported that patients with a history of alcohol abuse are more likely to be infected with HCV than the rest of the population (1).

In addition, ethanol has been suggested to exacerbate HCV-induced liver diseases in part by affecting the viral titer (2–5). Hepatitis C patients who drink alcohol typically show a pattern of hepatic injury that is more characteristic of chronic viral hepatitis than alcohol-induced injury, suggesting that alcohol enhances the pathogenic effects of HCV rather than exerting its independent effects on liver (6). Several clinical studies have correlated increased serum and intrahepatic HCV titer with the amount of alcohol consumed (2, 4, 5). Abstinence or moderation of alcohol consumption could reduce the HCV titer in some patients (2, 5). Furthermore, *in vitro* studies suggest that ethanol increases HCV RNA levels in Huh7 human hepatoma replicon cell lines that continuously support the HCV RNA replication without virus production (3, 7, 8). These studies suggest that ethanol enhances HCV replication both in the presence and absence of the complete viral replication cycle. HCV replicon systems and more recent virus-producing cell culture models have increased our understanding of HCV and provide us with tools for studying potential interactions between HCV and pathological cofactors, such as ethanol (9).

Nevertheless, whether ethanol directly enhances HCV production in the context of the complete viral replication cycle has not been demonstrated. Furthermore, the mechanism by which ethanol modulates HCV RNA replication remains controversial as reactive oxygen species (ROS) and lipid peroxidation products, which can be generated during ethanol metabolism, can suppress, rather than increase, HCV RNA replication in cells, suggesting the involvement of other metabolites of ethanol (10–14). Oxidative hepatic ethanol metabolism is a multistep process (4). Alcohol dehydrogenase, the predominant ethanol-metabolizing enzyme, is found in the cytosol and produces acetaldehyde and NADH. Ethanol-inducible cytochrome P450 (CYP2E1), which is induced during extended ethanol exposure, is another major ethanol-metabolizing enzyme located in the endoplasmic reticulum and generates NADP$^+$ and ROS in addition to acetaldehyde. Catalase, which is found in peroxisomes, is thought to not contribute significantly to ethanol metabolism under normal conditions. Once ethanol is metabolized into acetaldehyde, it is rapidly converted into acetate and NADH by aldehyde dehydrogenase. Acetaldehyde and other products of ethanol metabolism have been implicated in many pathogenic effects of ethanol. Whether these metabolites also

* This work was supported by start-up funds from the University of California, Merced (to J. C.).

[1] To whom correspondence should be addressed: School of Natural Sciences, University of California, Merced, 5200 N. Lake Rd, Merced, CA 95343. Tel.: 209-228-4386; Fax: 209-228-4060; E-mail: jchoi@ucmerced.edu.

[2] The abbreviations used are: HCV, hepatitis C virus; ROS, reactive oxygen species; nt, nucleotides; GAPDH, glyceraldehyde-3-phosphate dehydrogenase; qRT-PCR, quantitative reverse transcriptase-polymerase chain reaction; siRNA, small interfering RNA; IRES, internal ribosomal entry site; DADS, diallyl disulfide; BSO, L-buthionine *S,R*-sulfoximine; GSH, glutathione; GO, glucose oxidase; NAC, *N*-acetylcysteine; 4MP, 4-methylpyrazole; TOFA, 5-(tetradecyloxy)-2-furoic acid.

participate in the modulation of HCV replication by ethanol, however, has not yet been tested.

Therefore, the goal of this study was to determine the effects of ethanol exposure on HCV replication in the context of the complete HCV replication cycle and the mechanisms, comparing the effects of other metabolites of ethanol with those of ROS. Our data show that ethanol and acetaldehyde, at subtoxic and physiologically relevant concentrations, elevate complete HCV replication, as opposed to the suppression caused by endogenous and exogenous ROS. Our data further suggest that elevation of the ratio of NADH/NAD^+ and modulation of lipid metabolism are likely to play critical roles in the modulation of HCV replication by ethanol. Possible implications on *in vivo* HCV replication, patient education, and disease management are also discussed.

EXPERIMENTAL PROCEDURES

HCV Constructs—The genotype 2a HCV constructs, pJFH1 (produces infectious virus particles), replicative-null pJFH1-GND, and subgenomic pSgJFH1-Luc (contains a luciferase reporter gene), are described elsewhere (15, 16). Huh7 cell clones (SgPC2 and Clone B) supporting continuous replication of a subgenomic HCV replicon of genotype 1b (Con1 sequence) were also used (11, 17). The subgenomic replicons support HCV RNA replication but no virus is formed.

HCV RNA Transfection, Infection, and Cell Culture—The *in vitro* transcription, transfection of HCV RNA, and Huh7 human hepatoma cell culture were performed as described (10, 11). For the *in vitro* infectivity assays, 2 ml of the extracellular medium from JFH1 RNA-transfected cells were used to inoculate naïve Huh7 or Huh7.5 cells with 3 ml of fresh medium, as described (16, 18). Treatments were initiated 24 h after infection, and the cells were harvested after another 24 or 48 h.

Northern Blot Analysis—Intracellular RNA extraction and Northern blots were carried out, as described (10, 11). DNA probes were prepared from nucleotides (nt) 4128–8273 or 358–2816 of JFH1, generated with ScaI and ApaL I, respectively, or 3669 to 6016 of the Con1 subgenomic replicons. Images were quantified by densitometry, using Optiquant Cyclone 4.00 (Perkin Elmer), and data were normalized by glyceraldehyde-3-phosphate dehydrogenase (GAPDH) mRNA content.

Quantitative Real-time Reverse Transcriptase-Polymerase Chain Reaction (qRT-PCR)—The total intracellular RNA was obtained from cells using TRIzol (Invitrogen). To obtain extracellular HCV RNA, cell culture medium samples were first treated with RNase A (100 μg/ml) for 30 min at room temperature, then RNA was extracted using TRIzol LS, and glycogen as a carrier. HCV RNA was quantified by qRT-PCR as described (11, 16). The primer sequences for JFH1 were 5′-TCTGCGGAACCGGTGAGTA-3′ (nt 146–164; forward), and 5′-TCAGGCAGTACCACAAGGC-3′ (nt 277–295; reverse), and the sequence of the fluorogenic probe, labeled with 6-FAM and TAMRA (Biosearch Technologies, Inc.), was 5′-CCAGTCTTCCCGGCAATTCCG-3′ (nt 168–188). Standard curves were generated using *in vitro* transcribed HCV RNA. Intracellular HCV RNA levels were normalized by 18 S rRNA or GAPDH mRNA.

Western Blot Analysis—Cells were sonicated in Laemmli buffer, and proteins were analyzed for NS5A and β-actin by Western blot, as described (10). Loading was normalized by protein assay of acetone-precipitated proteins determined with the bicinchoninic acid assay kit (Pierce). Quantification of Western blots was performed by densitometry using the Kodak IS2000R software.

Luciferase Assays—After various treatments, SgJFH1Luc RNA-transfected cells were lysed with 1× Reporter Lysis Buffer, and the luciferase activity was determined using Luciferase Reporter Assay kit (Promega) (15). Luciferase activities were normalized by total protein content, determined with bicinchoninic acid assay kit (Pierce).

In Vitro HCV Replication Assay—In vitro replication assay was carried out, as previously described (10, 11). Briefly, cytoplasmic lysates were prepared, and the replication was allowed to proceed for 1 h at 30 °C in the presence of [α-^{32}P]CTP and actinomycin D. Then, RNA products were analyzed on a 1% formaldehyde-agarose gel, which was subsequently analyzed, using Optiquant Cyclone 4.00 (PerkinElmer Life Sciences).

CYP2E1 Small Interfering RNA (siRNA)—Huh7 and SgPC2 cells were transfected with 50 nM CYP2E1 (Santa Cruz Biotechnology) or non-targeting control (Dharmacon) siRNAs, using RNAiMax (Invitrogen) per the manufacturer's recommendations.

CYP2E1 Activity Assay—Cells were treated with and without 0.2% ethanol for 48 h and lysed. CYP2E1 activity was determined by measuring hydroxylation of *p*-nitrophenol as described, except NADPH, instead of the NADPH-generating system, was used (19). The specificity was demonstrated by inhibiting the reaction with 100 μM CYP2E1 antibodies, and portion of the activity that is inhibited by CYP2E1 antibodies was then calculated and reported.

NADH/NAD^+, Cholesterol, and ATP Assays—NADH and NAD^+ levels were determined by enzymatic NADH recycling assay, using the NAD^+/NADH Quantification kit from Biovision, per the manufacturer's recommendations. After various treatments, cells were collected in 400 μl of NADH/NAD^+ extraction buffer. Samples were immediately subjected to two freeze/thaw cycles and filtered using Microcon YM-10 (Millipore). Then, the samples were split into two sets, one of which was used to carry out the thermal decomposition of NAD^+ followed by the cycling assay for the determination of NADH content of the cell. The other set was used to measure the total NADH plus NAD^+ content by performing the cycling assay without the thermal decomposition. Then, the NADH/NAD^+ ratio was calculated. Total intracellular cholesterol was measured using the Cholesterol/Cholesteryl Ester Quantitation kit (Biovision) per the manufacturer's instructions. Briefly, cells were homogenized in chloroform/isopropyl alcohol/Triton X-100 (7:11:0.1). The lipids were extracted, and all traces of organic solvents were evaporated prior to resuspending the lipids in the reaction buffer and performing the assay. Total ATP content was measured using Somatic Cell ATP Assay kit (Sigma-Aldrich). The data were normalized by total protein content, determined with the bicinchoninic acid assay kit (Pierce).

Statistics—Data were analyzed using Student's *t* test or one-way analysis of variance, using SigmaStat 3.1 (Jandel Scientific).

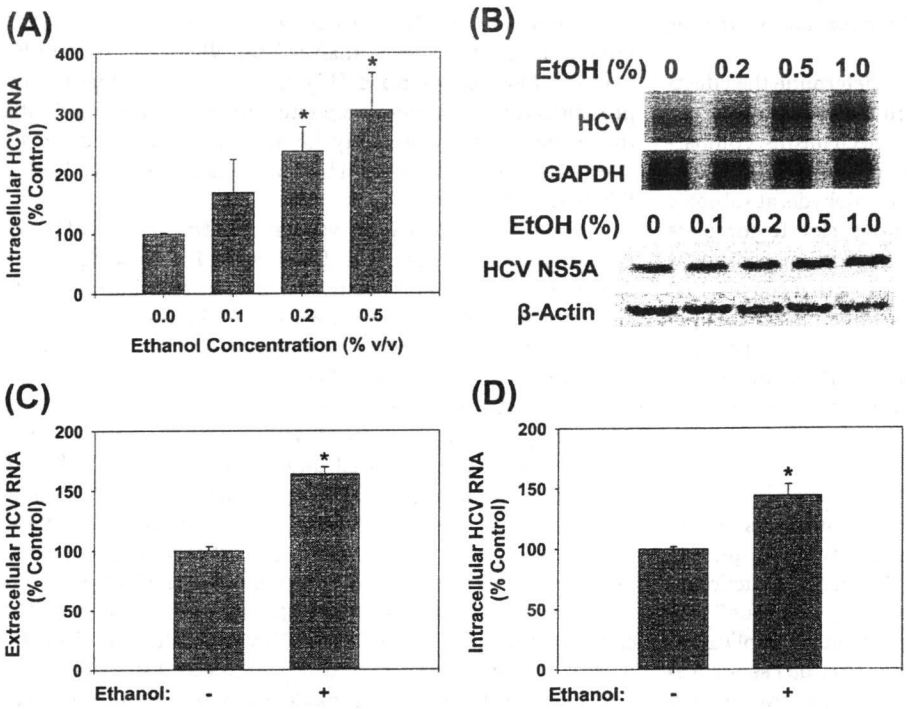

FIGURE 1. **Ethanol increases JFH1 replication.** Huh7 cells transfected with JFH1 RNA were analyzed for intracellular HCV RNA by (*A*) qRT-PCR ($n = 6$) or (*B*) Northern blots ($n = 4$) and for HCV NS5A protein content by Western blot ($n = 3$) (*B, bottom panel*) after 48 h of ethanol treatments. *C*, extracellular HCV RNA levels were analyzed by qRT-PCR for 0.2% ethanol treatments ($n = 4$). *D*, naïve Huh7 cells were inoculated with virus-containing medium and analyzed for HCV RNA after 48 h of 0.2% ethanol treatment ($n = 4$). *, indicates statistically significant difference for indicated sample sizes ($p < 0.05$).

A p value ≤ 0.05 was considered significant. All experiments were repeated three to six times, and either the means ± S.E. of several independent experiments or the representative Northern or Western blot images are shown.

RESULTS

Ethanol Increases the Complete Replication of HCV at Physiological Concentrations—To examine whether ethanol increased the complete replication of HCV, positive-sense genomic JFH1 RNA was produced by *in vitro* transcription using T7 RNA polymerase and transfected into Huh7 human hepatoma cells. Then, the transfected cells were exposed to 0–1.0% (v/v, 0–172 mM) ethanol once daily for 48 h. Then, the cells and the cell culture medium were harvested and analyzed for intracellular and RNase A-resistant extracellular HCV RNAs by a combination of Northern blots and qRT-PCR. Ethanol significantly increased the intracellular JFH1 HCV RNA levels to 237 ± 40 and 305 ± 61% of untreated controls at 0.2 and 0.5% concentrations, respectively ($p < 0.05$) (Fig. 1, *A* and *B, top panel*). HCV NS5A protein level similarly increased with ethanol treatments (Fig. 1*B, bottom panel*). Extracellular HCV RNA was also significantly elevated with the 0.2% ethanol treatment, indicating increased virus secretion (Fig. 1*C*). Next, we examined whether virus-infected cells responded similarly to ethanol treatment with elevated HCV RNA. We found that 0.2% ethanol also increased HCV RNA in Huh7 cells infected with cell culture-generated JFH1 virions (Fig. 1*D*). JFH1 GND mutant, which harbors a critical mutation (GDD:GND) in NS5B, the viral polymerase, did not replicate or generate infectious virus particles, as expected (data not shown). These concentrations of ethanol did not induce any cytotoxicity, as assessed by cell morphology and measuring the ATP content (data not shown). The 0.2% ethanol, equivalent to blood alcohol concentration of 34.4 mM, that significantly enhanced HCV replication, is approximately twice the legal limit for driving under the influence in many countries, including the United States. The 0.5% ethanol lies in the toxic range but can also be achieved physiologically, particularly in chronic alcohol users. In addition, ethanol is volatile, and the amount that remains would be significantly less than what was added to cell culture medium (20). These data, therefore, suggest that ethanol can enhance complete HCV replication, at physiologically attainable concentrations.

Ethanol Enhances HCV RNA Replication of Genotypes 2a and 1b—Previously, ethanol was shown to elevate HCV RNA content in Huh7 cells that supported subgenomic HCV RNA replication without virus production (3, 7, 8). To test whether the JFH1 RNA replication was also affected by ethanol, we transfected Huh7 cells with SgJFH1-Luc RNA and exposed the cells to ethanol for 48 h. Then, HCV replication was monitored by measuring the firefly luciferase activity (15). Ethanol increased the luciferase activity in these cells, suggesting that the JFH1 RNA genome replication was affected (Fig. 2*A*).

Genotype 2a HCV infection is found globally, with the prevalence ranging from less than 2 to about 30% depending on the geographical region (21, 22). However, as the most prevalent HCV genotype is genotype 1, we also repeated these experiments, using Con1 subgenomic replicon (SgPC2) cells (11, 17). Again, significant increases in the genotype 1b HCV RNA could be demonstrated with 0.1–1% ethanol (Fig. 2*B, top panel*). Similar increases in the HCV NS5A protein content was demonstrated by Western blots (Fig. 2*B, bottom panel*).

To confirm that the rate of the HCV RNA genome replication is accelerated by ethanol, we measured the activity of the HCV RNA replication complex. JFH1-transfected cells were exposed to ethanol for 5 h and then, the cytoplasmic lysates, containing the HCV replication complex, were isolated. Then, the *in vitro* RNA replication assay was performed in the presence of α-^{32}P-labeled CTP and actinomycin D, as previously described (11). JFH1 cell extracts produced a single band that corresponded to the expected size of the HCV RNA, indicating active viral RNA replication, whereas the JFH1 GND extracts did not (Fig. 2*C*). Ethanol significantly increased the rate of

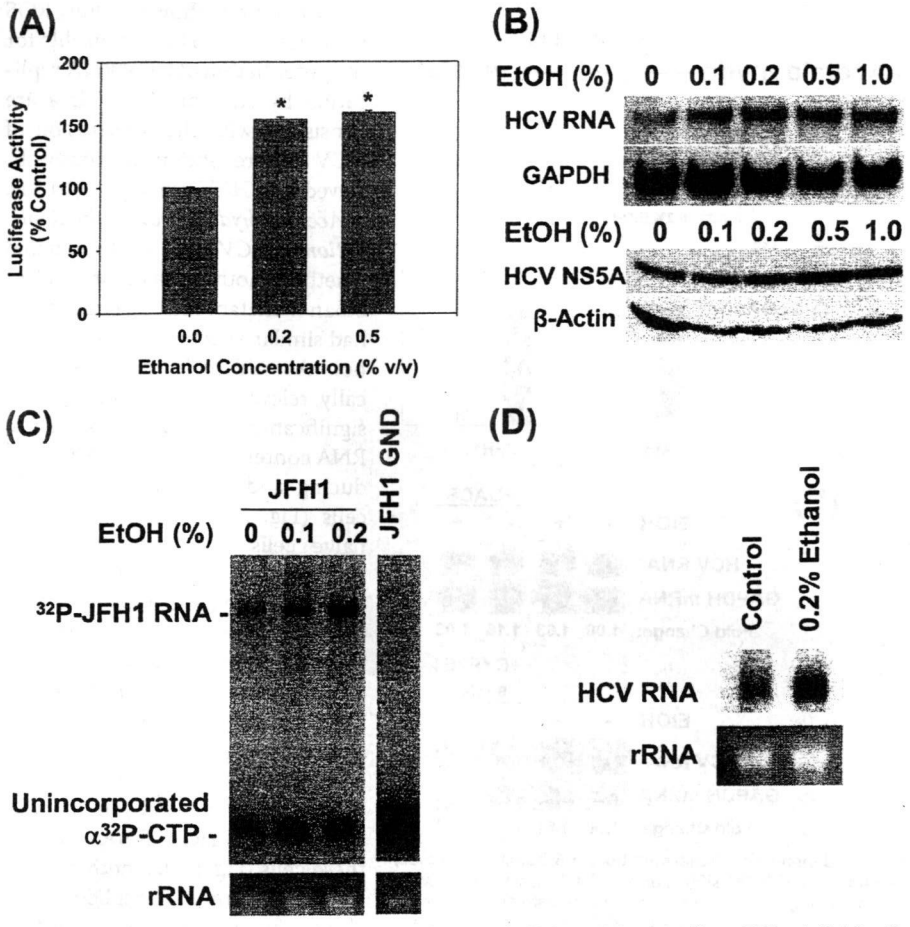

FIGURE 2. **Ethanol increases the replication of subgenomic JFH1 and Con1 replicon RNAs.** *A*, Huh7 cells transfected with SgJFH1-Luc RNA were analyzed for luciferase activity after 48-h ethanol treatments ($n = 3$). *B*, stable Huh7 clones expressing SgCon1-Neo (SgPC2) were incubated with ethanol for 24 h and analyzed for HCV RNA, GAPDH mRNA, and NS5A and β-actin proteins ($n = 3$) by Northern and Western blots, respectively ($n = 3$). *C* and *D*, cytosolic lysates were prepared from (*C*) JFH1 and JFH1-GND RNA-transfected cells and (*D*) SgPC2 cells, after 5 h of ethanol treatment, these lysates were used to carry out *in vitro* replication assays ($n = 3$). *Bottom panels* show ethidium bromide staining of rRNA as the loading control. *, indicates statistically significant difference for indicated sample sizes ($p < 0.05$).

HCV RNA replication (Fig. 2*C*). Ethanol also accelerated the *in vitro* replication rate of Con1 strain (Fig. 2*D*). On the other hand, ethanol did not increase the HCV internal ribosomal entry site (IRES) activity, as assessed by the HCV IRES activity assay, using pRL-HL (data not shown) (23). The data suggest that ethanol increases the rate of HCV RNA replication without directly enhancing its translation rate, at least when these processes are evaluated separately. Therefore, increases in the NS5A protein content with ethanol (Fig. 2*B*) are likely to have resulted from increased levels of the viral RNA template available for translation.

CYP2E1 Is Present in Huh7 Cells at Significant Levels as in Human Liver—Next, we started examining the mechanism by which ethanol increased HCV replication, first, by identifying key steps of ethanol metabolism that mediated this effect (Fig. 3*A*). Alcohol dehydrogenase I was not detected in significant levels in our Huh7 cells (data not shown). To confirm that ethanol metabolism is occurring in our cells, we then analyzed our Huh7 cells for the expression of CYP2E1. Our Huh7 cells expressed significant levels of CYP2E1 protein, which was about 2.2 ± 0.5-fold less than human liver (Fig. 3*B*). CYP2E1 expression could also be enhanced by 1.5 ± 0.2-fold with daily treatment with 0.2% (v/v) ethanol for 48 h (Fig. 3*C*). This enhanced expression of CYP2E1 could be maintained for at least 2 weeks. The CYP2E1 activities (Fig. 3*D*) were within the expected range for human liver, which is 0.25–3.3 nmol/min/mg protein, and paralleled the CYP2E1 expression levels (Fig. 3*C*) (19). CYP2E1 activity of human liver shown in Fig. 3*B* was 1.83 ± 0.01 nmol/min/mg. Con1 SgPC2 cells had similar expression and activity levels of CYP2E1 as Huh7 cells (0.81 ± 0.02 nmol/min/mg without ethanol; 1.01 ± 0.06 nmol/min/mg with 0.2% ethanol).

The ethanol-induced potentiation of HCV replication could be abrogated with 25 μM diallyl disulfide (DADS), an inhibitor of CYP2E1 (Fig. 3*E*). In addition, CYP2E1 siRNA, which decreased CYP2E1 protein level to 35 ± 9% ($p < 0.05$) of the controls transfected with non-targeting control siRNA, also significantly blunted the potentiation of HCV replication by ethanol (Fig. 3*E*). These data suggest that ethanol is being metabolized by these cells, and that CYP2E1 activity is critical for the potentiation of HCV replication by ethanol in our system.

ROS Suppresses JFH1 Replication—Hepatic ethanol, particularly CYP2E1-mediated, metabolism generates ROS in addition to acetaldehyde (24) (Fig. 3*A*) and previously, we showed that ROS could suppress subgenomic Con1 and H77c/Con1 hybrid HCV RNA replication in these cells (10, 11). To resolve these seemingly conflicting observations, we continued to examine how ROS affected JFH1. To examine the effects of endogenously generated ROS, we first used L-buthionine *S,R*-sulfoximine (BSO). BSO depletes glutathione (GSH), a major endogenous antioxidant, by inhibiting its *de novo* synthesis. Therefore, BSO would amplify the effects of endogenous ROS, generated during normal cellular metabolism and in response to HCV (4). BSO decreased intracellular GSH content by ~80 ± 12% in Huh7 cells ($p < 0.05$). In addition, BSO decreased both intracellular and extracellular JFH1 RNA levels (Fig. 4, *A* and *B*). To confirm that BSO was acting specifically by decreasing GSH, cells were treated with BSO and GSH ethyl ester, which enters cells and is cleaved by cellular esterases to restore GSH inside cells, bypassing the inhibition of GSH biosynthesis by BSO. GSH ethyl ester partially restored both intracellular and extracellular HCV RNA (Fig. 4, *A* and *B*).

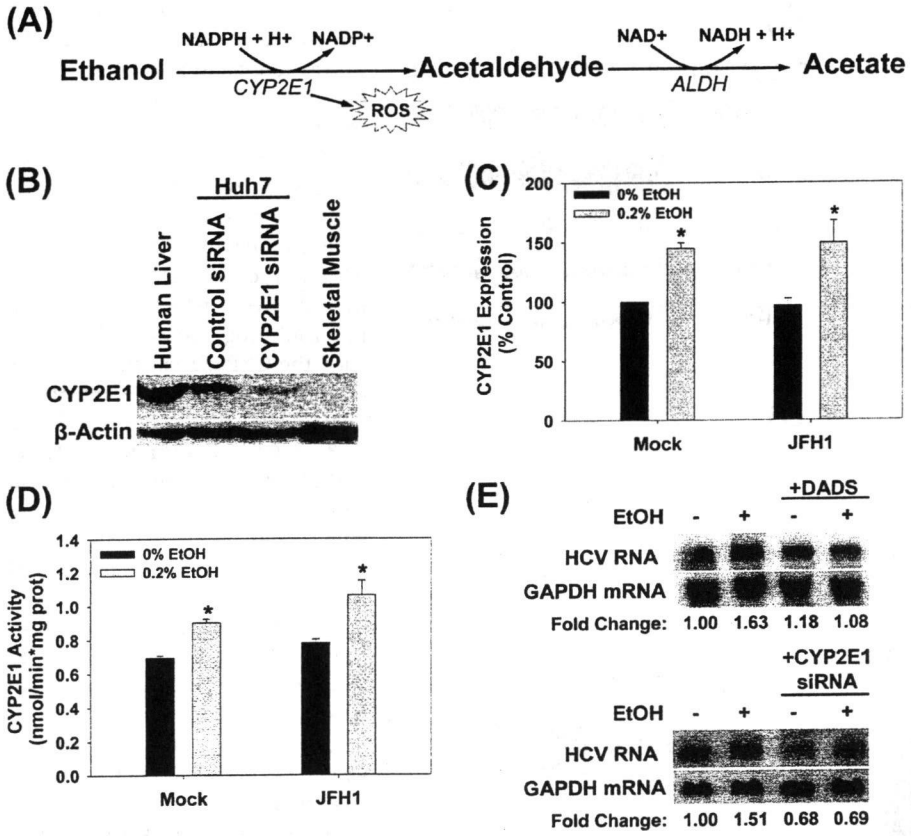

FIGURE 3. **CYP2E1 expression in Huh7 cells.** *A*, CYP2E1-dependent ethanol metabolism. *B*, human liver tissue, Huh7 cells transfected with 50 μM non-targeting control or CYP2E1 siRNA, and skeletal muscle tissue were analyzed for CYP2E1 protein content by Western blot ($n = 3$). *C* and *D*, mock- or JFH1-transfected Huh7 cells were incubated with or without 0.2% (v/v) ethanol for 48 h and analyzed for (*C*) CYP2E1 expression by Western blot ($n = 3$) and (*D*) CYP2E1-dependent *p*-nitrophenol hydroxylation activity ($n = 3$). *E*, SgPC2 cells were exposed to 0.2% ethanol ± 25 μM DADS for 24 h or transfected with 50 nM control or CYP2E1 siRNA for 24 h and then incubated with ethanol for 24 h and analyzed for HCV RNA by Northern blot ($n = 3$). *, indicates statistically significant difference for indicated sample sizes ($p < 0.05$).

assay (data not shown). Thus, ROS were not likely to be responsible for the potentiation of HCV RNA replication by ethanol. These data are consistent with the suppression of HCV RNA replication previously observed with HCV genotype 1 (10, 11).

Acetaldehyde Increases the Replication of HCV—We next evaluated whether another major product of ethanol metabolism, acetaldehyde, had similar effects on HCV as ethanol. Acetaldehyde, at physiologically relevant concentrations (25), significantly increased the HCV RNA content in both non-virus producing and virus-producing JFH1 cells (Fig. 5, *A* and *B*). Infecting naïve cells with virus-containing medium and then treating with 5 μM acetaldehyde also led to significant increases in HCV replication (Fig. 5*C*). To examine whether acetaldehyde had similar effects on genotype 1b HCV, SgPC2 cells were also incubated with acetaldehyde and analyzed for changes in HCV replication. Acetaldehyde likewise elevated the HCV RNA level in these cells (Fig. 5*D*). Another Con1 HCV subgenomic replicon cell clone, Clone B, derived in another laboratory (17), responded similarly to ethanol and acetaldehyde, indicating that the response is not specific to our cell clone (Fig. 5*D*). Thus, acetaldehyde is sufficient to potentiate HCV replication of both genotypes 1b and 2a.

Isopropyl Alcohol and Acetone Also Potentiate HCV Replication, the Role of NADH/NAD$^+$—We continued to investigate whether acetaldehyde itself or products of acetaldehyde metabolism are critical for the potentiation of HCV replication by ethanol by inhibiting aldehyde dehydrogenase with cyanamide (see Fig. 3*A*). Cyanamide suppressed the potentiation of HCV replication by ethanol just as inhibiting the first step of ethanol metabolism with 4-methylpyrazole (4MP) and DADS did, suggesting that it is not acetaldehyde itself but a downstream product of acetaldehyde metabolism that increases HCV replication (Fig. 6*A*, *left panel*).

Acetaldehyde metabolism by aldehyde dehydrogenase generates NADH and acetate (Fig. 3*A*). To determine the potential role of NADH, we first evaluated the effects of isopropyl alcohol. Isopropyl alcohol (0.2%, v/v) increases the levels of NADH like ethanol but generates acetone instead of acetaldehyde. To our surprise, isopropyl alcohol also increased the HCV RNA level (Fig. 6*B*, *left panel*) (26). Both isopropyl alcohol and ethanol increased NADH/NAD$^+$ ratio in these cells, as expected

Adding extracellular GSH, which is broken down into its constituents, then taken up for intracellular *de novo* GSH synthesis, and does not bypass the BSO-inhibited step, could not restore the HCV RNA level in these cells, as expected. The data suggest that BSO decreases HCV replication specifically by decreasing GSH.

To examine the effects of the exogenous ROS, JFH1 RNA-transfected cells were incubated with 0.25 milliunits/ml of glucose oxidase (GO), which produces H_2O_2 extracellularly through an enzymatic reaction in the presence of glucose, mimicking ROS generation during inflammation. GO decreased the intracellular JFH1 RNA by 30 ± 8% ($p < 0.05$) and exacerbated the suppression of HCV RNA by BSO (Fig. 4*C*). In addition, JFH1 RNA levels decreased with 25, 50, and 100 μM H_2O_2 (Fig. 4*D*). Treating cells with BSO plus GO or either agent alone likewise suppressed the subgenomic JFH1 RNA replication (Fig. 4*E*). BSO and H_2O_2 also countered the enhancement of HCV replication by ethanol (Fig. 4*F*). Furthermore, *N*-acetylcysteine (NAC) and Trolox, a water soluble vitamin E, either increased or had no significant effect on the ethanol-induced enhancement of HCV replication (Fig. 4*G*). These cell treatments did not induce cytotoxicity, as determined by the ATP

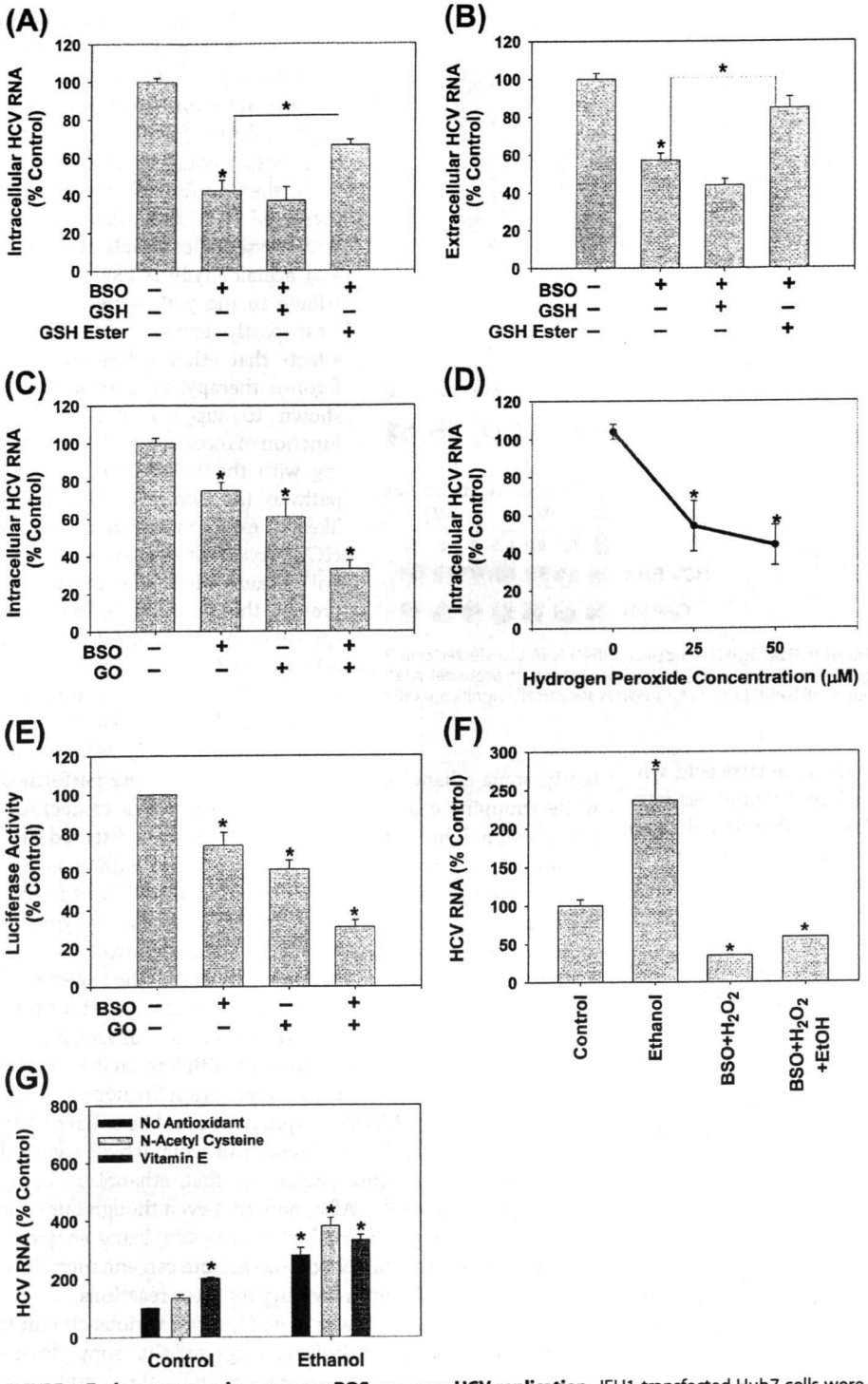

FIGURE 4. **Endogenous and exogenous ROS suppress HCV replication.** JFH1-transfected Huh7 cells were treated with BSO with and without 2 mM GSH or GSH ester (*A* and *B*) ($n = 3$), GO + glucose with and without 16 h of pretreatment with 20 μM BSO (*C*) ($n = 4$), or bolus H_2O_2 (*D*) ($n = 4$) for 24 h. Then, JFH1 intracellular (*A*, *C*, *D*) and extracellular (*B*) HCV RNA levels were analyzed by qRT-PCR. *E*, Huh7 cells transfected with SgJFH1-Luc RNA were assayed for luciferase activity after 24 h treatment with 0.25 milliunits/ml glucose oxidase + glucose with and without the BSO pretreatment ($n = 3$). *F*, SgPC2 cells were treated with 0.2% ethanol ± H_2O_2 plus BSO for 24 h, and analyzed for HCV RNA and GAPDH mRNA by Northern blot. *G*, SgPC2 cells were treated for 24 h with ethanol ± 5 mM NAC or 0.5 μM Trolox (water-soluble vitamin E). Then, HCV RNA and GAPDH mRNA levels were monitored by Northern blot and quantified by densitometry ($n = 3$). *, indicates statistically significant difference for indicated sample sizes ($p < 0.05$).

(Fig. 6*B*, *right panel*). In contrast, *tert*-butanol did not elevate HCV replication or the NADH/NAD^+ ratio (Fig. 6*B*).

Moreover, we found that acetate itself increased the level of HCV RNA as treating cells with acetone also did. In addition, ethanol, acetaldehyde, acetate, isopropyl alcohol, and acetone all showed corresponding increases in NADH/NAD^+ ratios (Fig. 6*B*, *right panel*) (4, 27). The NADH/NAD^+ ratios were positively correlated with HCV RNA content in all of these treatments ($r = 0.95$, $p < 0.001$) (Fig. 6*B*). The suppression of HCV replication by cyanamide, 4MP, and DADS in Fig. 6*A* (*left panel*) was also associated with corresponding decreases in the NADH/NAD^+ ratios (Fig. 6*A*, *right panel*). Therefore, changes in HCV replication paralleled the changes in the NADH/NAD^+ ratio, produced by these treatments.

Then, we examined whether increased NADH/NAD^+ ratio was required for the potentiation of HCV replication by ethanol and these other agents. Pyruvate, which re-oxidizes cytosolic NADH to NAD^+, completely abrogated the increases in HCV replication and NADH levels during ethanol, acetaldehyde, acetate, isopropyl alcohol, and acetone treatments (Fig. 6*C*). Methylene blue, which also oxidizes NADH, had similar effects on HCV as pyruvate (data not shown). In contrast, lactate, which produces NADH in the cytosol independent of ethanol, increased NADH levels to 235.9 ± 11.9% ($p < 0.05$) of the control level but had little to no effect on HCV replication (Fig. 6*D*). Together, these data indicate that whereas an alteration of cellular NADH/NAD^+ levels seems necessary for the ethanol-induced increases in HCV replication, elevated NADH/NAD^+ may not be sufficient to increase HCV replication.

The Potentiation of HCV Replication by Ethanol Requires Lipogenesis—NADH has diverse functions in the cell, and one of these functions includes modulation of lipid metabolism. For example, NADH can

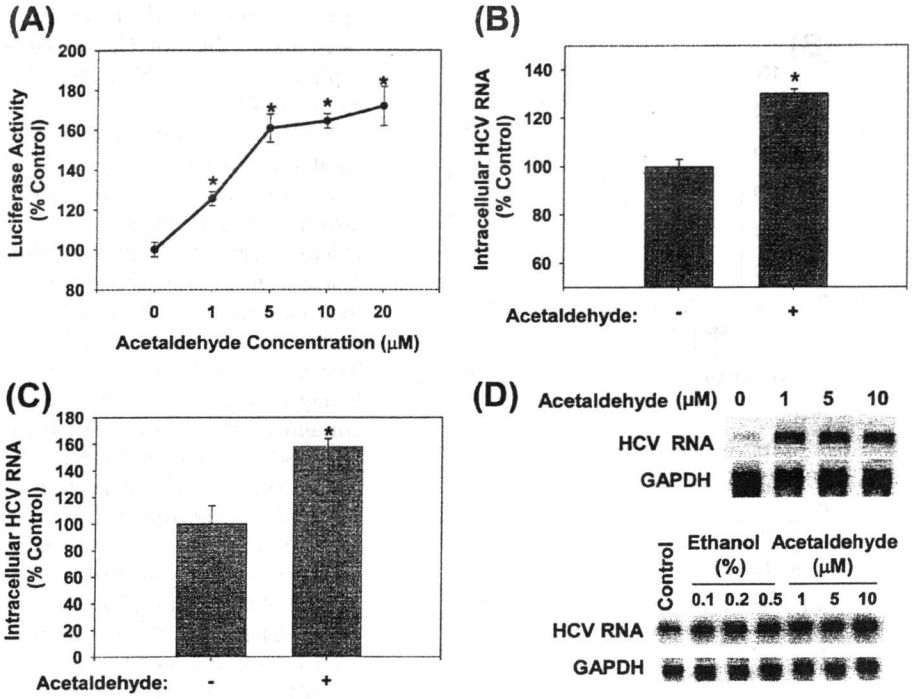

FIGURE 5. **Acetaldehyde increases intracellular HCV RNA.** SgJFH1-Luc (*A*) and JFH1 RNA-transfected cells (*B*), Huh7.5 cells inoculated with JFH1 virions (*C*), SgPC2 and Clone B cells (*D*) were incubated with acetaldehyde for 24 h and analyzed for HCV RNA by Northern blot or qRT-PCR ($n = 3$). *, indicates statistically significant difference for indicated sample size ($p < 0.05$).

inhibit mitochondrial β-oxidation and increase fatty acid synthesis (28). It is well-established that ethanol modulates fatty acid metabolism in part through NADH, and that this plays an important role in the development of steatosis in the alcoholic liver (28). Acetate and acetone would generate acetyl-CoA, which also drives lipogenesis (27, 28). Furthermore, cholesterol metabolism and fatty acid biosynthesis are important in HCV RNA replication (29). Lovastatin and fluvastatin, which are competitive inhibitors of 3-hydroxy-3-methyl-glutaryl-CoA reductase, and 5-(tetradecyloxy)-2-furoic acid (TOFA) and cerulenin, which inhibits fatty acid biosynthesis, have been shown to suppress the basal level of HCV replication (29, 30). Therefore, we next examined whether the potentiation of HCV RNA replication by above agents might be inhibited by modulators of lipid metabolism.

Lovastatin, fluvastatin, TOFA, and cerulenin almost completely inhibited the potentiation of HCV RNA replication by ethanol, acetaldehyde, isopropyl alcohol, acetone, and acetate (Fig. 7, *A* and *B*). In addition, inhibiting β-oxidation of fatty acids with β-mercaptopropionic acid caused a 15.2 ± 1.7-fold ($p < 0.01$) increase in HCV replication in these cells (Fig. 7*C*). Furthermore, ethanol, acetaldehyde, acetone, and acetate treatments increased the total intracellular cholesterol content, which was attenuated by lovastatin (Fig. 7*D*). Lactate, which increased NADH/NAD^+ without increasing HCV replication, had no significant effect on cholesterol levels (Fig. 7*D*). The data suggest that the elevation of HCV replication by ethanol, acetaldehyde, acetone, and acetate is mediated by increases in intracellular cholesterol and can be abrogated by the inhibition of cholesterol or fatty acid biosynthetic pathways.

DISCUSSION

High HCV titer is associated with the development and progression of liver diseases (31). In addition, ethanol consumption, high BMI, and high viral titer are strongly associated with poor response to anti-HCV therapy (32). Therefore, the increased HCV replication we saw with physiological levels of ethanol and acetaldehyde is likely to contribute to the pathogenesis and at least partly explain the negative effects that ethanol has on interferon-α therapy. Ethanol has been shown to suppress the antiviral function of interferon-α by interfering with the JAK-STAT signaling pathway (33); however, this is not likely to explain the potentiation of HCV replication we saw with ethanol because HCV effectively suppresses the type I interferon response in Huh7 cells. Additionally, ethanol and acetaldehyde could increase HCV replication in RIG-I-defective Huh7.5 cells (Fig. 5*C*, also, data not shown) (18, 34). Importantly, some ethanol treatments in this study were performed while wrapping cell culture dishes with parafilm to decrease loss of ethanol due to evaporation. However, we observed similar potentiation of HCV replication by ethanol, with and without the parafilm. The use of the parafilm also did not induce hypoxia as no significant change in the expression of hypoxia-inducible factor-1α could be found (data not shown).

Previously, it has been suggested that some of the key ethanol metabolizing enzymes might not be expressed in Huh7 cells (33). Indeed, we also found that alcohol dehydrogenase I is decreased in our Huh7 cells compared with human liver. However, CYP2E1 activity of our cells were within the normal range for human liver, and CYP2E1 expression could be enhanced by ethanol (Fig. 3). In addition, ethanol and acetaldehyde elevated the NADH/NAD^+ ratio, indicating that ethanol is being metabolized by our cells. Also, note that even though our cells do not have all of the normal ethanol metabolizing enzymes, our discovery that acetaldehyde and acetate can enhance HCV replication is significant as they bypass these reactions.

A previous study by Zhang *et al.* (3) using various chemical inhibitors of ethanol metabolism, suggested that some downstream metabolites of ethanol were involved in the potentiation of subgenomic HCV RNA replication by ethanol. Our data are in agreement with this study and suggest that ethanol and acetaldehyde also directly enhance HCV replication in the context of the complete viral replication cycle. In terms of the mechanism, we found that isopropyl alcohol, acetone, and acetate also increase HCV replication, and increased NADH/NAD^+ ratio was required for the potentiation of HCV replication by etha-

nol, acetaldehyde, as well as isopropyl alcohol, acetone, and acetate. In contrast, *t*-butanol, a tertiary alcohol that is poorly metabolized by humans and does not increase the NADH/NAD^+ ratio, did not elevate HCV replication, as predicted by our model (Fig. 6*B*). The NADH/NAD^+ ratio in ethanol-treated cells was decreased by cyanamide (Fig. 6*A*), suggesting that NADH is generated downstream of acetaldehyde (Fig. 3*A*). Acetate, the downstream metabolite of acetaldehyde, was previously considered inert but there is evidence that it can be converted to acetyl-CoA and other metabolic intermediates by mammalian cells (24, 28). Isopropyl alcohol is known to be metabolized into acetone and possibly other ketone bodies that can also be converted to acetyl-CoA (27). The mechanism by which isopropyl alcohol increases the NADH/NAD^+ ratio in our system is unclear and may involve residual ADH or hitherto uncharacterized enzyme activity that is induced by HCV.

In terms of how NADH increases HCV replication, NADH plays key roles in cellular bioenergetics and can modulate fatty acid synthesis as well as suppress β-oxidation (24, 28). We were interested in the potential involvement of lipids because HCV replicates in cholesterol-rich compartments in the cell, and cholesterol and fatty acid metabolism have been shown to be important for HCV replication (29). Specifically, cholesterol metabolism increases basal HCV replication by the geranylgeranylation of FBL2 (29). We found that inhibiting the host mevalonate pathway with statins and fatty acid synthesis with TOFA or cerulenin blunted the potentiation of HCV replication by ethanol, acetaldehyde, isopropyl alcohol, acetone, and acetate, whereas inhibiting β-oxidation dramatically increased HCV replication (Fig. 7). In addition, the potentiation of HCV replication by these agents was accompanied by an increase in the intracellular cholesterol content, which was attenuated by lova-